

1 **Coherent activity at three major 2 lateral hypothalamic neural outputs 3 controls the onset of motivated 4 behavior responses**

5 **Ekaterina Martianova^{1*}, Alicia Pageau¹, Nikola Pausic¹, Tommy Doucet
6 Gentiletti¹, Danahe Leblanc¹, Christophe D. Proulx^{1*}**

*For correspondence:

christophe.proulx@fmed.ulaval.ca

7 ¹CERVO Brain Research Center, Department of Psychiatry and Neuroscience, Université
8 Laval, Québec, Canada

10 **Abstract**

11 The lateral hypothalamus (LH) plays an important role in motivated behavior. However, it is not
12 known how LH neural outputs dynamically signal to major downstream targets to organize
13 behavior. We used multi-fiber photometry to show that three major LH neural outputs projecting
14 to the dorsal raphe nucleus (DRN), ventral tegmental area (VTA), and lateral habenula (LHb)
15 exhibit significant coherent activity in mice engaging motivated responses, which decrease during
16 immobility. Mice engaging active coping responses exhibit increased activity at LH axon terminals
17 that precedes an increase in the activity of serotonin neurons and dopamine neurons, indicating
18 that they may play a role in initiating active responses stemming from LH signal transmissions.
19 The optogenetic activation of LH axon terminals in either the DRN, VTA, or LHb was sufficient to
20 increase mobility but had different effects on passive avoidance and sucrose consumption,
21 suggesting that LH outputs use complementary mechanisms to control behavioral responses.
22 Our results support the notion that the three LH neural outputs play complementary roles in
23 initiating motivated behaviors.

24

25 **Introduction**

26 An animal that wishes to maximize its survival must select optimal behavioral responses in order to
27 correctly adapt to its environment. Deciding to execute or refrain from a specific action depends
28 largely on the actual state of the environment that needs to be accurately integrated and then
29 translated into adaptive responses (*Tye, 2018; Verharen et al., 2020*). In other words, an animal
30 will engage active behavioral responses to obtain a reward, avoid a punishment, or escape from
31 an aversive context. Alternatively, it can engage passive coping behaviors to avoid being seen by a
32 predator or to avoid exhaustion.

33 The lateral hypothalamus (LH) is a heterogeneous brain region that has been associated with
34 a variety of behaviors related to motivation, reward, stress, arousal, and feeding (reviewed in *Bon-*
35 *navion et al. (2016)* and *Fakhoury et al. (2020)*). More recently, its role in reward processing has
36 been explored, specifically in innate defensive behaviors and in signaling aversive stimuli and the
37 cues that promote them (*González et al., 2016a; Hassani et al., 2016; Noritake and Nakamura,*
38 *2019; Karnani et al., 2020; Lecca et al., 2017; Trusel et al., 2019; de Jong et al., 2019*).

39 Recent studies investigating individual LH neural outputs have shown that LH neuronal out-

40 puts to the lateral habenula (LHb) and the dopaminergic (DA) ventral tegmental area (VTA) play
41 important roles in these processes. LH neurons projecting to the lateral habenula (LH→LHb) are
42 activated by aversive stimuli and encode cue-predicting aversive stimuli to motivate escape and
43 avoidance (*Lecca et al., 2017; Trusel et al., 2019; Stamatakis et al., 2016*). LH projections to the
44 dopaminergic ventral tegmental area (VTA) also play important roles in motivating compulsive re-
45 ward seeking (*Nieh et al., 2015*), controlling innate defensive behaviors, and providing information
46 on aversive outcomes (*de Jong et al., 2019*).

47 The dorsal raphe nucleus (DRN) is another brain center that plays an important role in reward
48 processing and motivated behaviors (*Nakamura, 2013*). Direct activation of serotonergic (5-HT,
49 5-hydroxytryptamine) DRN neurons increases active coping behavior (*Nishitani et al., 2019*), that
50 originates from the prefrontal cortex and the LHb transmission (*Warden et al., 2012; Amat et al.,
51 2001; Dolzani et al., 2016*). The DRN receives profuse projections from the LH (*Weissbourd et al.,
52 2014; Pollak Dorocic et al., 2014; Zhou et al., 2017; Ogawa and Watabe-Uchida, 2018*). Interestingly,
53 pharmacological modulation of LH activity has been shown to exert either positive or negative con-
54 trol of serotonergic DRN neurons (*Celada et al., 2002*), suggesting that it is involved in control-
55 ling DRN activity. However, the function of LH projections to the DRN in live behaving animal is
56 unknown.

57 The LH, LHb, VTA and DRN are interconnected brain nuclei (*Weissbourd et al., 2014; Pollak
58 Dorocic et al., 2014; Zhou et al., 2017; Ogawa and Watabe-Uchida, 2018; Stamatakis et al., 2016;
59 Lazaridis et al., 2019; Lecca et al., 2017*). However, it not known how these structures are dynami-
60 cally engaged to control behavior. Here, we used multi-fiber photometry (*Martianova et al., 2019*)
61 to simultaneously monitor neural activity at LH axon terminals in three major brain targets. Our re-
62 sults show that largely non-overlapping LH neuronal populations transmit coherent signals to the
63 DRN, VTA, and LHb. Activity along these pathways is coincident with the onset of motivated behav-
64 ior responses. We also show that activity at LH axon terminals precedes activity at serotonergic
65 neurons in the DRN (*DRN^{5HT}*) and dopaminergic neurons in the VTA (*VTA^{DA}*). While optogenetic
66 stimulation of LH terminals in the DRN, VTA, and LHb increased active coping behavior, it had a dif-
67 ferent effect on sucrose consumption, suggesting that these pathways play complementary roles
68 in controlling behavior responses. Taken together, our results show that the three major LH neural
69 outputs play complementary roles in engaging motivated behaviors.

70 Results

71 **The LH→DRN, LH→VTA, and LH→LHb pathways are activated by aversive airpuffs 72 and inhibited during sucrose consumption**

73 To simultaneously examine activity at the LH→DRN, LH→VTA, and LH→LHb pathways (*Figure 1A*),
74 we injected an adeno-associated virus (AAV) encoding the calcium indicator GCaMP6s (AAV-CAG-
75 GCaMP6s) in the LH of wild-type mice. Optical fibers were implanted over the DRN, VTA, and LHb,
76 allowing us to monitor activity at LH axon terminals projecting to the DRN, VTA, and LHb, respec-
77 tively (*Figure 1B*). Four weeks post-injection, GCaMP6s expression was detected in the cell bodies
78 of the LH and in the axon terminals of these fibers in the DRN, VTA, and LHb (*Figure 1B*). Calcium-
79 dependent changes in fluorescence at axon terminals, which is a proxy for neural activity, was
80 recorded simultaneously in all three pathways using multi-fiber photometry in freely behaving
81 mice (*Figure 1C*) (*Martianova et al., 2019*). To directly compare the neural dynamics of these three
82 LH neural outputs, the mice were placed in an open-field arena, and 1-s airpuffs (aversive stimulus)
83 were delivered on top of the animals every 60 s (*Figure 1D*). *Figure 1E* shows representative traces
84 where spontaneous activity was detected at all three pathways, which significantly increased co-
85 incidentally with the delivery of the airpuffs (*Figure 1F*). Control mice injected with an AAV-eYFP
86 exhibited no significant changes in fluorescence following the delivery of airpuffs (*Figure 1–Figure
87 Supplement 1C*) indicating that changes in fluorescence are dependent on changes in calcium and
88 GCaMP6s signals and do not result from movement artifacts.

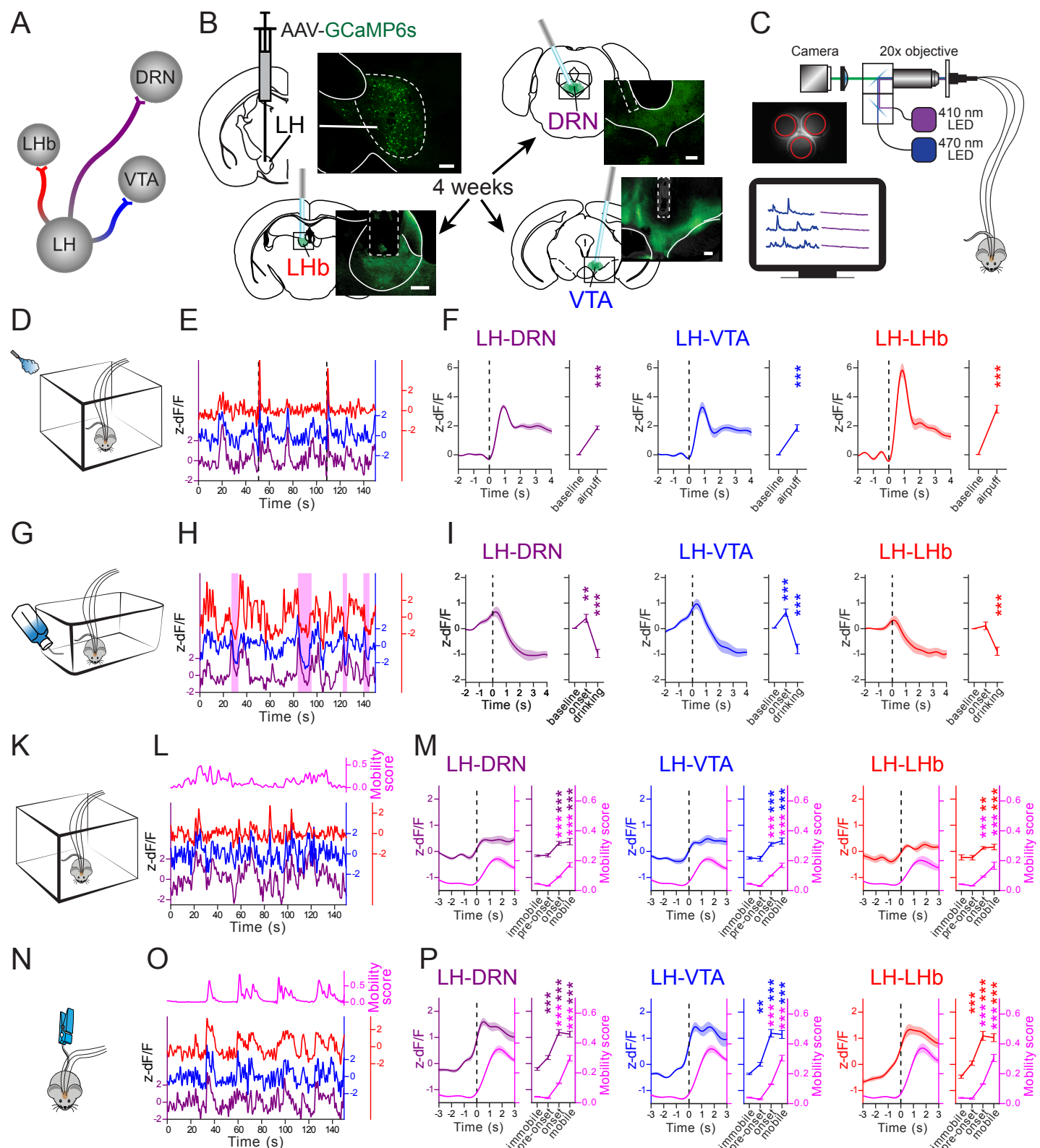


Figure 1. The LH \rightarrow DRN, LH \rightarrow VTA, and LH \rightarrow LHb pathways are activated by airpuffs, at onset of mobility and are inhibited during sucrose consumption. **(A)** Diagram of the LH neural outputs targeted in this work. **(B)** Diagram of the experimental setup and fluorescence images of GCaMP6s expression in LH neurons and axon terminals at the DRN, VTA, and LHb (scale bar 200 μm). **(C)** Diagram of the multi-fiber photometry calcium (Ca^{2+}) imaging setup. **(D)** Experimental setup for the airpuffs. **(E)** Representative Ca^{2+} signal traces associated with the airpuffs (dashed vertical bars) simultaneously measured at the LH \rightarrow DRN, LH \rightarrow VTA, and LH \rightarrow LHb pathways. **(F)** Peri-event plot of the average Ca^{2+} signal traces with all airpuff events at the LH \rightarrow DRN, LH \rightarrow VTA, and LH \rightarrow LHb axon terminals. Plot of area under the curve (AUC) before and after the airpuffs. The lines represent means \pm SEM (standard error of mean).

Figure 1. Same convention as with **D-F** for the sucrose consumption test (**G-I**), the open field test (**K-M**), and the tail suspension test (**N-P**). Sucrose consumption events are represented by pink shaded box in **H**. The magenta lines are mobility scores. Repeated measures three-way ANOVA between factors group (GCaMP6s- and eYFP-expressing mice) and within factors pathway (LH→DRN, LH→VTA, and LH→LHb), and time period (different for each test) with post hoc Dunnett's test. The *p* values were adjusted using the Bonferroni multiple testing correction method. **p* < 0.05, ***p* < 0.01, ****p* < 0.001.

Figure 1-Figure supplement 1. Recordings from the LH→DRN, LH→VTA, and LH→LHb pathways in control eYFP-expressing mice.

Figure 1-Figure supplement 2. Pearson correlation between the signals recorded at the LH→DRN, LH→VTA, and LH→LHb pathways in mice expressing GCaMP6s and eYFP.

Figure 1-Figure supplement 3. Cannulae placement in the mice expressing GCaMP6s

Figure 1-Figure supplement 4. Cannulae placement in the mice expressing eYFP

Figure 1-Figure supplement 5. The LH neural populations projecting to the DRN, VTA, and LHb are largely distinct populations.

Figure 1-Figure supplement 6. Ca^{2+} imaging from the LH neurons projecting to the DRN and the VTA

Figure 1-Figure supplement 7. The cannulae placement in mice prepared using the intersectional viral strategy

Figure 1-source data 1. fig1_LH_apt-sct-oft-tst.xlsx contains AUC from APT, SCT, OFT, and TST experiments with mice expressing GCaMP6s and correlation analysis between outputs; related to figure 1 and figure supplement 2.

Figure 1-source data 2. fig1-supp1_LH-eYFP.xlsx contains AUC from all experiments with control mice expressing eYFP and correlation analysis between outputs; related to figure supplement 1 and 2.

Figure 1-source data 3. fig1-supp6_LHretro.xlsx contains AUC from all experiments with mice prepared using intersectional viral strategy; related to figure supplement 6.

Figure 1-source data 4. Fig1_stats.ipynb contains statistical analysis related to figure 1 and its supplements.

89 To investigate how these pathways are modulated in an appetitive context, the same mice were
90 water-deprived for 24 h and were then given free access to a 2% sucrose solution for 10 min (**Figure 1G**). In these sessions of sucrose consumption (SCT), the mice readily learned to drink from
92 the sucrose dispenser. Drinking events were automatically detected with a lickometer, and are
93 represented by pink boxes in the representative traces shown in **Figure 1H**). Aligning the signals
94 with the onset of drinking events revealed that activity at the LH→DRN and LH→VTA pathways in-
95 creased significantly immediately prior to the onset of sucrose consumption, indicating that these
96 pathways play a role in initiating motivated goal-directed behavior. This change was not seen with
97 the LH→LHb pathway. In all three pathways, however, activity significantly decreased during su-
98 crose consumption (**Figure 1G**). No specific changes in the signal at the onset of or during sucrose
99 consumption were observed in eYFP-expressing control mice (**Figure 1-Figure Supplement 1F**).

100 **A Coherent increase in activity at the LH→DRN, LH→VTA, and LH→LHb pathways
at the onset of mobility**

102 Previous studies have shown that the LH→VTA and LH→LHb pathways play a role in motivating de-
103 fensive behaviors. However, our results suggest that the LH neural outputs may also play a role in
104 controlling spontaneously motivated behavior. For example, the mice fled when given an aversive
105 airpuff, increased their mobility to reach a drinking spout, and stayed put during consumption.

106 To directly examine the role of LH neural outputs in motivated behavior, activity was measured
107 at LH neural outputs and movements were tracked with an automated ANY-maze video tracking
108 system. The mice were free to explore either an open field (OFT) (**Figure 2A-C**) or were suspended
109 by the tail (tail suspension test, TST) (**Figure 2D-F**). OFT and TST are neutral and stressful contexts,
110 respectively, and presumably engage different motivational drives to move. **Figure 1L** and O show
111 representative activity traces monitored at the LH neural outputs and superimposed on the mobil-
112 ity score (magenta line), of a mouse placed in the open field or a mouse suspended by its tail, re-
113 spectively. In these contexts, activity at the LH→DRN, LH→VTA, and LH→LHb pathways significantly
114 increased at mobility onset. In addition, mice placed in the TST exhibited a significant increase in
115 activity at all three LH neural outputs immediately prior to the onset of mobility. A Pearson cor-
116 relation analysis confirmed the coherence between these pathways, which we did not observe in
117 eYFP-expressing mice (**Figure 1-Figure Supplement 2**). Taken together, these results show that

118 these three major LH neural outputs exhibit coherent activity.

119 **Distinct LH neuronal populations project to DRN, VTA, and LHb**

120 The coherence observed at the LH neural outputs could be explained if there were extensive collat-
121 eral projections from the LH to the DRN, VTA, and LHb. To determine whether LH neural outputs
122 send out significant collateral projections, we first injected the same mouse with three fluorescently
123 labeled retrograde markers in the DRN, VTA, and LHb. Three to four days later, we performed a
124 histological analysis and quantified LH neurons that were positive for one or more fluorescent
125 markers (*Figure 1–Figure Supplement 5*). Our analysis revealed largely non-overlapping LH neu-
126 ronal populations projecting either to the DRN, the VTA, or the LHb, with less than 5% of LH neu-
127 rons being positive for two or three fluorescent markers. This observation is consistent with a
128 previous report showing that distinct LH neural outputs projecting to VTA, LHb and dPAG (*de Jong*
129 *et al.*, 2019). To further determine whether the activity measured at LH axon terminals was from
130 distinct LH populations, we used an intersectional viral approach to express the red-shifted cal-
131 cium sensor jrGECO1a (*Dana et al.*, 2016), and GCaMP6s in DRN- and VTA-projecting LH neurons,
132 respectively (*Figure 1–Figure Supplement 6A*) (*Martianova et al.*, 2019; *Kakava-Georgiadou et al.*,
133 2019). To this end, AAV vectors with retrograde properties (*Tervo et al.*, 2016), encoding the cre
134 or FlpO recombinase were injected into the DRN and the VTA, respectively. A cre-dependent AAV
135 encoding jrGECO1a (AAV-DIO-jrGECO1a) and a FlpO-dependent AAV encoding GCaMP6s (AAV-fDIO-
136 GCaMP6s) were injected into the LH of the same mice. As with fluorescent retrograde markers, this
137 approach mainly labelled non-overlapping, and distinct LH neuronal populations (*Figure 1–Figure*
138 *Supplement 6A*). An optical fiber was implanted over the LH of these mice to monitor signals from
139 jrGECO1a and GCaMP6s expressed in DRN- and VTA-projecting LH neurons by dual-color fiber pho-
140 tometry (*Martianova et al.*, 2019). When the mice were tested using the same behaviors described
141 above, the calcium signals perfectly replicated the results previously obtained from the axon ter-
142 minals recordings. These results indicate that the LH sends out largely independent projections,
143 that it signals to the DRN, VTA and LHb, and that this activity is coherent to mobility onset.

144 **Increased activity at the LH→DRN, LH→VTA, and LH→LHb pathways precedes cop- 145 ing responses**

146 A Pearson correlation analysis between LH neural output activity and mobility score measured with
147 the OFT and TST showed a significant positive correlation, with the exception of the LH→LHb path-
148 way with the OFT (*Figure 2A*), indicating that these pathways play a role in controlling movement.
149 This correlation was significantly higher with the TST, an aversive context engaging active and pas-
150 sive coping responses (*Commons et al.*, 2017). To further investigate whether the high correlation
151 between activity and the mobility score could be attributed to specific time events during the OFT
152 and TST, we performed peri-event correlation analyses at specific time points (events). Events of
153 four types were chosen: at mobility onset, at immobility onset, and at random time points during
154 mobility and immobility. For each event, a Pearson correlation was measured for each 6-seconds
155 peri-event traces of the mobility score and the calcium signal recorded at each of the LH outputs.
156 Correlations with $p < 0.001$ and $r > 0.6$ were considered as positive correlation events, $p < 0.001$
157 and $r < 0.6$ as negative correlation events, and the others events as having no correlation. The
158 number of positive, negative, and no correlations events were counted for each mouse, each time
159 event, and each behavior test. The means \pm SEM for all of the animals are given in *Figure 2C*.
160 The statistical analysis revealed that the main difference between the groups was the number of
161 positive correlations. The results were independent of the output (no difference by this factor or
162 interactions with others). In other words, the number of positive correlations events was similar
163 for the LH→DRN, LH→VTA, and LH→LHb pathways. This analysis revealed that the number of pos-
164 itive events was significantly higher at mobility onset and during mobility in the TST than in the OFT.
165 The highest number of positive correlations events was observed at mobility onset during the TST.
166 A cross-correlation analysis between activity and mobility score also revealed that changes in ac-

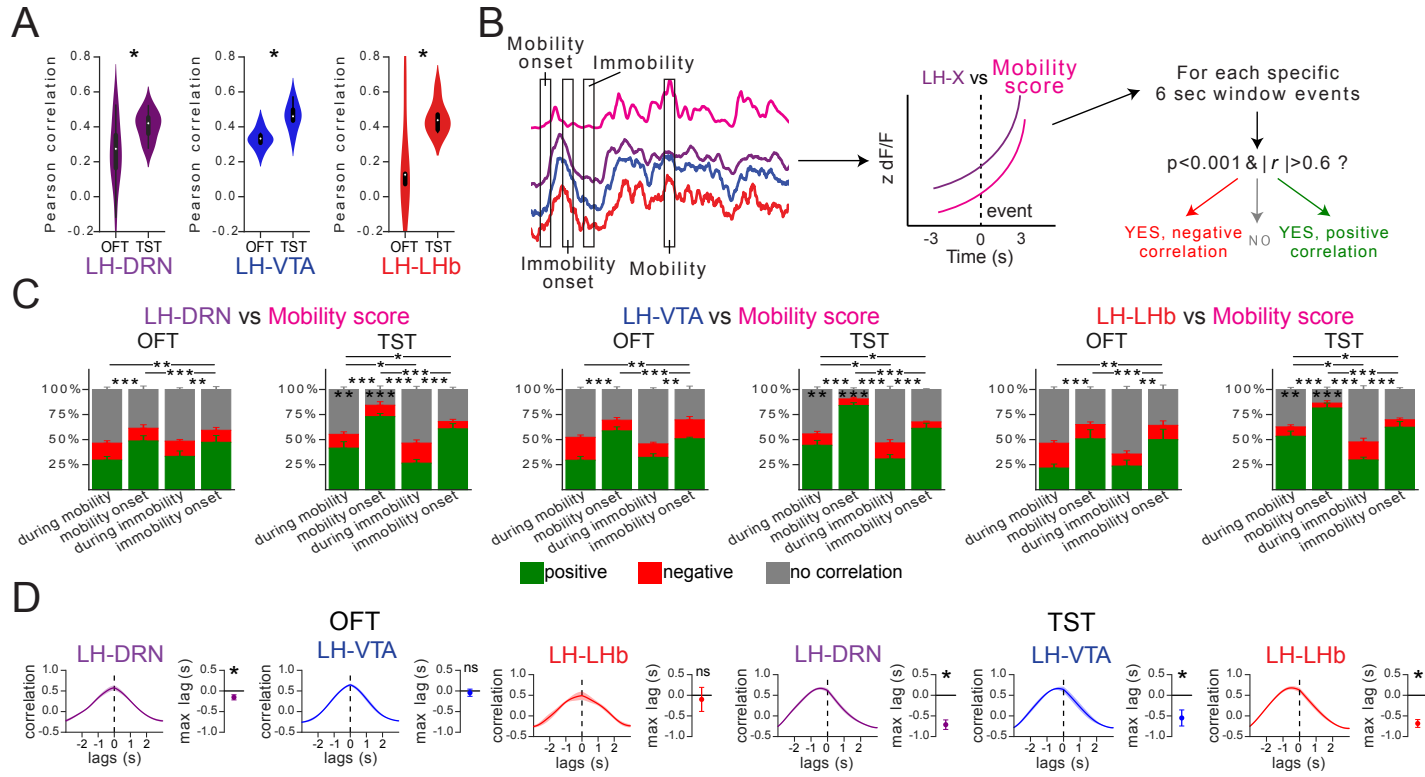


Figure 2. There was a high correlation between activity and mobility score at the LH \rightarrow DRN, LH \rightarrow VTA, and LH \rightarrow LHb pathways during the TST. **(A)** Pearson correlation between Ca^{2+} signal at the LH \rightarrow DRN, LH \rightarrow VTA, and LH \rightarrow LHb pathways, and mobility scores during the OFT or TST. One sample t-test. Three-way mixed ANOVA between factors group (GCaMP6s- and eYFP-expressing mice), and within factors test (OFT and TST) and pathways (LH \rightarrow DRN, LH \rightarrow VTA, and LH \rightarrow LHb) with post hoc Tukey test. The p values were adjusted using the Bonferroni multiple testing correction method. **(B)** Schematic of the event selection. Events at the onset mobility and immobility, and random events during mobility and immobility were chosen, and the Pearson correlation at 6 seconds peri-events between the Ca^{2+} signal and the mobility score was calculated. Correlations with $p < 0.001$ and $r > 0.6$ were considered as positive, $p < 0.001$ and $r < 0.6$ as negative, and the others as uncorrelated. **(C)** Fraction of positive (green), negative (red), and uncorrelated events (gray) in the OFT and TST for the LH \rightarrow DRN, LH \rightarrow VTA, and LH \rightarrow LHb pathways. Four-way MANOVA between the factors group (GCaMP6s- and eYFP-expressing mice), test (OFT and TST), and pathways (LH \rightarrow DRN, LH \rightarrow VTA, and LH \rightarrow LHb), and within factor events (during mobility, mobility onset, during immobility, immobility onset) for positive and negative correlations with a post hoc four-way mixed ANOVA and Tukey test for multiple comparisons. The p values were adjusted using the Bonferroni multiple testing correction method. The main effect was due to differences in the number of positive correlations. There was no difference in factor output and its interactions with other factors. Asterisks on the bars show the difference between tests. **(D)** Cross-correlation analysis between the Ca^{2+} signal and the mobility score at mobility onset peri-events. The lines represent means \pm SEM of correlations vs. lag times and means \pm SEM of lag times with maximum correlation. One sample t-test. Two-way ANOVA within factors tests (OFT and TST) and pathways (LH \rightarrow DRN, LH \rightarrow VTA, and LH \rightarrow LHb) with post hoc Tukey test. The p values were adjusted using the Bonferroni multiple testing correction method. * $p < 0.05$, ** $p < 0.01$, *** $p < 0.001$.

Figure 2-Figure supplement 1. Correlation analysis between the signal at one of the LH neural output pathways and mobility score in mice expressing eYFP.

Figure 2-source data 1. fig2_LH_movementCorrelation.xlsx contains correlation results of GCaMP6s-expressing mice; related to figure 1.

Figure 2-source data 2. fig2_LH-eYFP_movementCorrelation.xlsx contains correlation results of eYFP-expressing mice; related to figure 1.

Figure 2-source data 3. Fig2_stats.ipynb contains statistical analysis related to figure 2 and its supplements.

167 tivity from all three LH neural outputs preceded the change in mobility at mobility onset when the
168 mice initiated an active coping response in the TST (**Figure 2D**). These results indicate that there is
169 a significant correlation in activity between these three LH neural outputs, and suggest that activity
170 at these LH neural outputs controls motivated behavior, particularly to engage a coping response
171 in a stressful context.

172 **Increased activity at LH axon terminals precedes increased activity of serotonin
173 and dopamine neurons**

174 To determine whether the change in activity measured at LH axon terminals was correlated with a
175 postsynaptic change in activity, we have performed dual-color fiber photometry recordings of LH
176 axon terminals while co-monitoring the activity of serotonin and dopamine neurons in the DRN
177 and VTA respectively. To this end, a cre-dependent AAV encoding jrGECO1a (AAV-DIO-jrGECO1a)
178 was injected into the DRN of ePet-cre mice, or in the VTA of DAT-ires-cre mice. These are transgenic
179 mouse lines exclusively expressing the recombinase cre in 5-HT neurons (*Scott et al., 2005*) and
180 DA neurons (*Bäckman et al., 2006*), respectively. AAV-GCaMP6s was also injected into the LH of
181 the same mice, and optical fibers were implanted in the DRN and the VTA as described above (**Fig-
182 ure 3A, D**). Four weeks post-injection, GCaMP6s expression was observed in the LH axons terminals
183 and jrGECO1a expression was observed in the cell bodies of 5-HT neurons (Tph2+) and DA neurons
184 (TH+) in the DRN and VTA, respectively (**Figure 3–Figure Supplement 1A, D**). This approach allowed
185 us to simultaneously monitor activity in LH axons terminals (green fluorescence from GCaMP6s)
186 and in genetically-defined 5-HT and DA neurons (red fluorescence from jrGECO1a) using the same
187 optical fiber. Representative traces show spontaneous activity from LH axon terminals as well as
188 from DRN^{5HT} and VTA^{DA} neurons. The activity at DRN^{5HT} neurons significantly increased with aver-
189 sive airpuffs and decreased during sucrose consumption, replicating the results from the LH axon
190 terminals (**Figure 3–Figure Supplement 1B, E**). However, the activity of VTA^{DA} neurons increased sig-
191 nificantly with aversive airpuffs and during sucrose consumption (**Figure 3–Figure Supplement 1C,
192 F**). When evaluated by the OFT and TST, the activity of VTA^{DA} neurons increased significantly at
193 the onset of mobility in the TST, but not in the OFT (**Figure 3B, C**). However, the activity of DRN^{5HT}
194 increased significantly at mobility onset in both tests (**Figure 3E, F**). In addition, the activation of
195 DRN^{5HT} and VTA^{DA} neurons was preceded by the activation of the LH→DRN and the LH→VTA path-
196 ways (**Figure 3C, F**). These results confirm that axon terminal activity is correlates with the postsy-
197 naptic activity of DRN^{5HT} and VTA^{DA} neurons, suggesting that the LH may be an important relay
198 for transmitting signals to serotonergic and dopaminergic nuclei in order to engage motivated
199 behaviours in aversive contexts.

200 **The LH→DRN, LH→VTA, and LH→LHb pathways are activated by aversive cues**

201 The LH→VTA and LH→LHb pathways encode aversive cues for active defensive behaviors (*Barbano
202 et al., 2020; de Jong et al., 2019; Trusel et al., 2019*). To determine whether the LH→DRN pathway
203 play a complementary role, we trained mice using an active avoidance task while simultaneouly
204 monitoring activity at LH terminals in the DRN, VTA and LHb. The mice learned to associate a
205 conditioned stimulus (CS) predicting an upcoming mild foot shock that could be escaped or avoided
206 by crossing from one compartment to the other of the two-compartment box (**Figure 4A**). The mice
207 quickly learned to avoid foot shocks, with the mean escape latency decreasing and the fraction
208 of avoidance increasing in the late phase of training (**Figure 4B**). Activity at the LH→DRN, LH→VTA,
209 and LH→LHb pathways was monitored during the early and late stages of learning. Mobility scores
210 were calculated using the DeepLabCut software package for markerless animal pose estimations
211 (*Mathis et al., 2018*). Our results show that activity following the aversive cue during late training
212 increases significantly in all three LH pathways, suggesting that learning signals are encoded in
213 these pathways. Activity increased further at the onset of the foot shock and the escape response
214 during early and late training (**Figure 4C**). We then investigated activity in trials where avoidance
215 occurred, with the mice avoiding the foot shock by shuttling to the other compartment of the two-

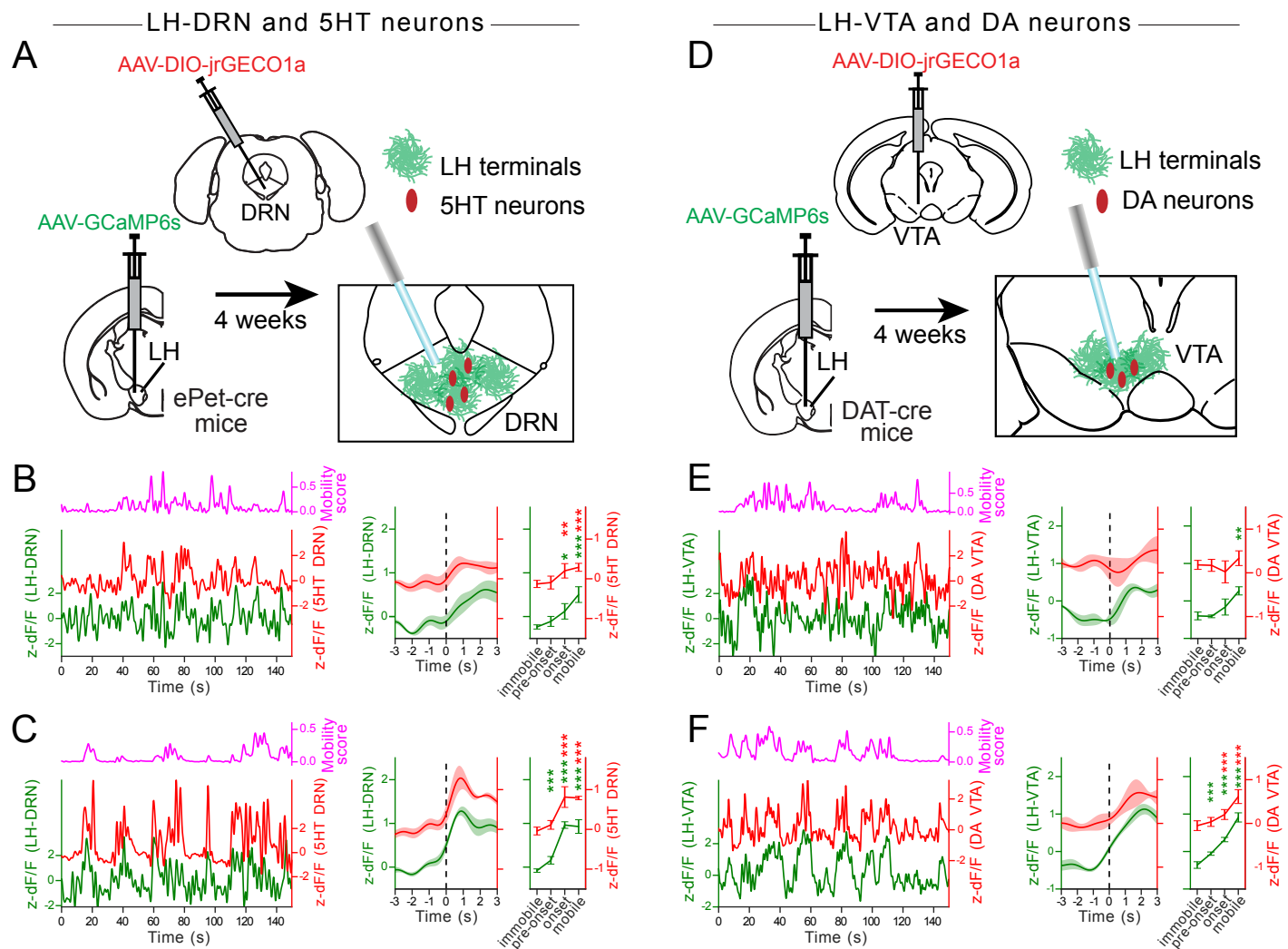


Figure 3. Increased activity of DRN^{5HT} and VTADA neurons follows increased activity in the LH→DRN and LH→VTA pathways at mobility onset in the TST. **(A, D)** Diagrams of the experimental setups for simultaneous recordings from the DRN^{5HT} neurons and the LH→DRN pathway **(A)** and from the VTADA neurons and the LH→VTA pathway **(D)**. **(B, E)** Representative Ca^{2+} signal traces from the DRN^{5HT} neurons and the LH→DRN pathway **(B)** and the VTADA neurons and the LH→VTA pathway **(E)** during the OFT **(left)**. Peri-event plots of the average Ca^{2+} signals at all mobility onsets and plots for AUC during immobility and mobility, and at mobility pre-onset and onset **(right)**. The lines represent the means \pm SEM (standard error of mean). Same convention as with **B, E** for the TST **(C, F)**, the magenta lines are mobility scores. Repeated measures two-way ANOVA within factors pathways (DRN^{5HT} and LH→DRN, or VTADA and LH→VTA) and time periods (during immobility and mobility, at mobility pre-onset and onset) with post hoc Dunnett's test. The *p* values were adjusted using the Bonferroni multiple testing correction method.

p* < 0.05, *p* < 0.01, ****p* < 0.001.

Figure 3-Figure supplement 1. Simultaneous recordings at the DRN^{5HT} neurons and the LH→DRN pathway, and at the VTADA neurons and the LH→VTA pathway in the AP and the SCT.

Figure 3-Figure supplement 2. Cannulae placement in the ePet-cre and the DAT-ires-cre mice.

Figure 3-source data 1. fig3_5HT.xlsx contains AUC from all experiments with ePet-cre mice; related to figure 3A-C figure supplement 1A-C.

Figure 3-source data 2. fig3_DA.xlsx contains AUC from all experiments with DAT-ires-cre mice; related to figure 3D-F figure supplement 1D-F.

Figure 3-source data 3. Fig3_stats.ipynb contains statistical analysis related to figure 3 and its supplements.

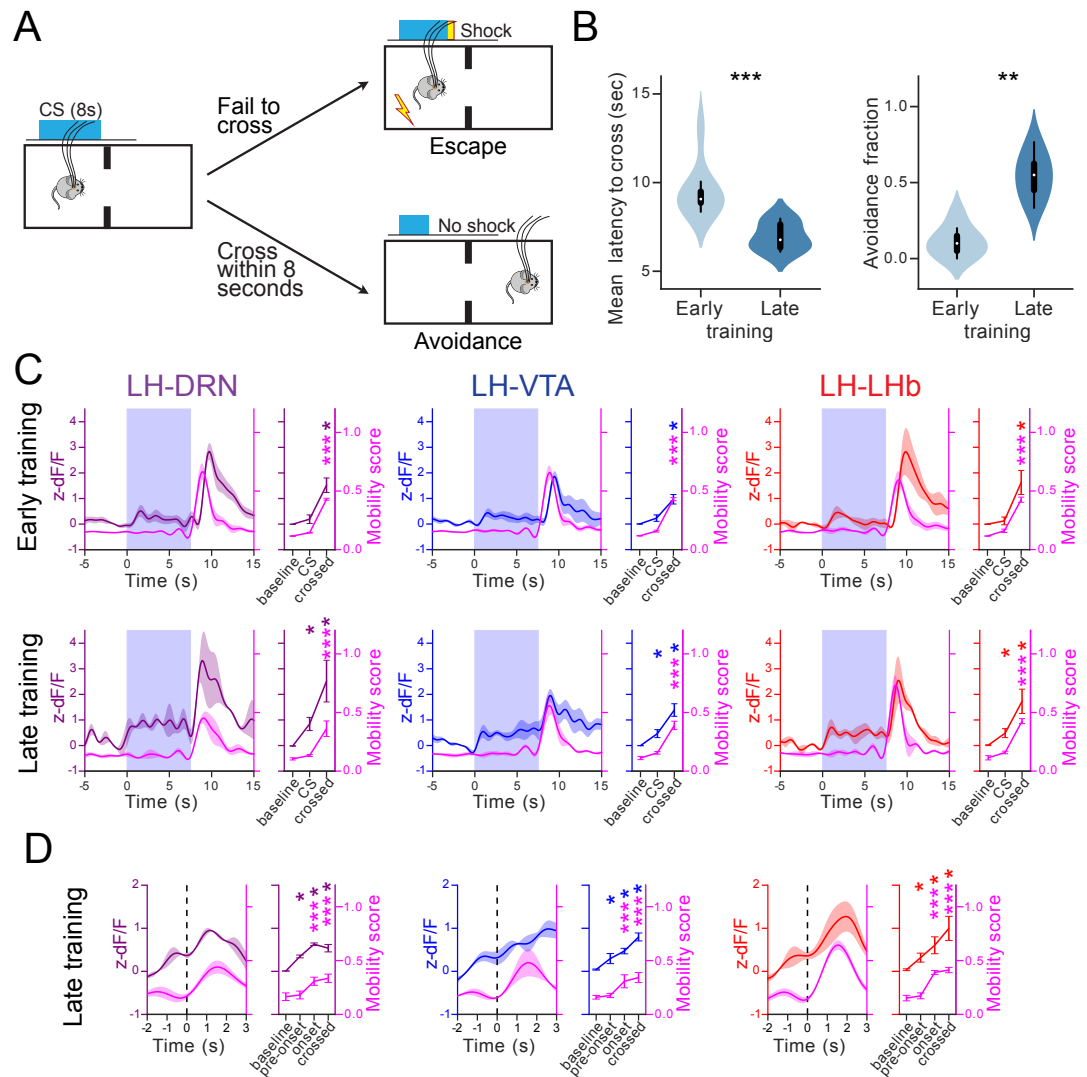


Figure 4. The LH→DRN, LH→VTA, and LH→Lhb pathways are activated by aversive cues **(A)** Diagram of the avoidance conditioning test. The mice learn to shuttle within 8 second of conditioned stimuli (CS, tone and light) in order to avoid a foot-shock. **(B)** The difference between early and late training trials is represented by the latency in shuttling from one compartment of the box to the other and the fraction of avoidance. **(C)** Peri-event plots of average Ca^{2+} signals to all CS events followed by escape at the LH→DRN, LH→VTA, and LH→Lhb axonal terminals and plots for AUC at baseline, during CS and escape. The lines represent means \pm SEM. The **top** plots represent the results during early training and the **bottom** plots represents the results during late training. Same convention as **C** for mobility onsets of avoidance during late training **D**. The magenta lines are mobility scores. Two-way repeated measures ANOVA within factors pathways (LH→DRN, LH→VTA, and LH→Lhb) and time periods (different for CS and mobility onset) with post hoc Dunnett's test. The p values were adjusted using the Bonferroni multiple testing correction method. * $p < 0.05$, ** $p < 0.01$, *** $p < 0.001$.

Figure 4-Figure supplement 1. Cannulae placement.

Figure 4-source data 1. fig4_LH_avoidanceTask.xlsx contains AUC from avoidance task with GCaMP6s-expressing mice; related to figure 4.

Figure 4-source data 2. Fig4_stats.ipynb contains statistical analysis related to figure 4.

216 compartment box before receiving the foot shock. We observed a significant increase in peri-event
217 activity at onset of avoidance in all three pathways, which provides further support for their role
218 in engaging self-motivated responses (*Figure 4D*), reminiscent of what we observed with the TST.

219 **The LH provides monosynaptic excitatory and inhibitory inputs to serotonergic
220 and non-serotonergic neurons in the DRN**

221 Previous studies have shown that LH neurons control the LHb through excitatory inputs while send-
222 ing both excitatory and inhibitory projections to the VTA, differentially targeting dopaminergic and
223 GABAergic neurons (*de Jong et al., 2019; Barbano et al., 2016, 2020; Nieh et al., 2016*). To examine
224 synaptic transmission from the LH to DRN, the LH of wild-type mice were injected with AAV-ChR2-
225 eYFP. Three weeks later, acute brain slices encompassing the DRN were prepared, and whole-cell
226 responses were obtained from DRN neurons. All the recordings were made in the presence of TTX
227 and 4-AP to avoid polysynaptic responses. Recorded neurons were filled with biocytin and were
228 identified as serotonergic or non-serotonergic by post hoc staining for tryptophane hydroxy-
229 lase (TPH). In voltage-clamp mode recordings, 5-ms light pulses evoked excitatory inward currents
230 and inhibitory outward currents at -60 mV and 0 mV holding currents, respectively. Monosynaptic
231 excitatory and inhibitory transmissions were blocked with the AMPA receptor antagonist NBQX and
232 the GABA-a receptor antagonist gabazine, respectively. In whole-cell current clamp mode record-
233 ings with a -30 mV depolarized voltage and in presence of TTX and 4-AP, single light pulse induced
234 a small depolarization followed by a large hyperpolarization. In the presence of gabazine however,
235 the single light-pulses revealed a large excitatory depolarizing component. No major difference
236 were observed between serotonergic and non-serotonergic DRN neurons (not shown). These
237 results confirm that LH sends convergent monosynaptic excitatory and inhibitory inputs to the
238 DRN (*Zhou et al., 2017*), and suggest that LH inhibitory transmission gate excitatory transmission
239 on both serotonergic and non-serotonergic neurons in the DRN.

240 **Optostimulation of the LH→DRN, LH→VTA, and LH→LHb pathways increases mo-
241 bility**

242 To determine whether increased activity at LH neural outputs is sufficient to motivate behavior, the
243 LH of wild-type mice were injected with an AAV encoding the opsin Channelrhodopsine-2 (ChR2)
244 fused to the fluorescent protein eYFP (AAV-ChR2-eYFP), or with eYFP alone (AAV-eYFP) as a control.
245 Optical fibers were implanted as described for the fiber photometry recordings (*Figure 6A*). A single
246 optical fiber cannula was connected to a 450-nm laser light source for the optogenetic stimulation
247 of individual LH neural outputs. All three LH neural outputs were tested using a Latin square ex-
248 perimental design, with 24 h between experimental sessions. The mice were subjected to 20-min
249 TST sessions. Each session consisted of 2-min epochs with or without 5-ms light pulses delivered in
250 20Hz optical stimulation trains (*Figure 6B*). The stimulation of individual LH neural outputs was suf-
251 ficient to increase mobility during the 2-min stimulation epochs compared to the non-stimulation
252 epochs in the TST (*Figure 6C*). The stimulation had no effect on the mobility of mice expressing eYFP
253 only (*Figure 6D*). The same results were also obtained in the OFT (*Figure 6-Figure Supplement 1*).
254 These results show that increased activity at individual LH neural outputs is sufficient to promote
255 motivated behavior.

256 **Optostimulation of LH neural outputs has distinct effects in place preference and
257 sucrose consumption**

258 Consistent with previous studies, we found that the stimulation of the LH→LHb pathway was
259 aversive. The mice avoided a context paired with the stimulation during a real-time place pref-
260 erence (RTPP) test (*Figure 7-Figure Supplement 1A-B*). However, even though the stimulation of
261 the LH→DRN and LH→VTA pathways significantly increased mobility in the TST and OFT, it did not
262 promote place preference or place avoidance in the RTPP. To further investigate the contribution

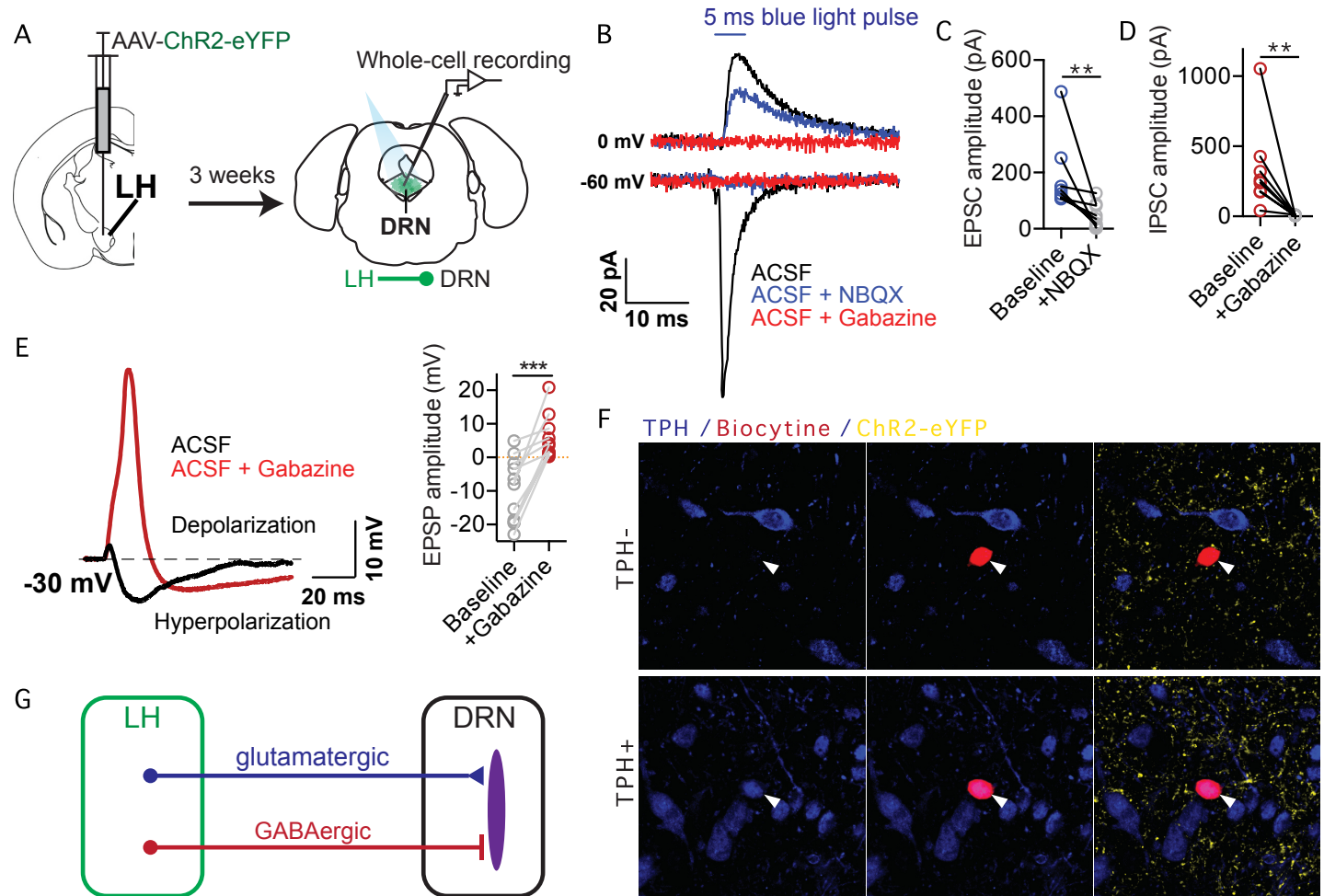


Figure 5. The LH provides monosynaptic excitatory and inhibitory projections to serotoninergic and non-serotoninergic neurons in the DRN. **(A)** Diagram of the experimental setup. **(B)** Representative monosynaptic response from a DRN neuron following optogenetic stimulation of LH axon terminals. The response involves both an excitatory inward current measured at -60 mV and an inhibitory outward current measured at 0 mV, which were respectively blocked by the AMPA receptor antagonist (NBQX, blue) and the GABA-a receptor antagonist (gabazine, red). Plots of ChR2-evoked EPSCs (**C**) and IPSCs (**D**) before and after blockade with the respective antagonists. **(E)** Representative monosynaptic response from a DRN neuron at a -30 mV holding voltage following optogenetic stimulation of LH axon terminals (left), and plots of EPSP amplitudes before and after GABA-a receptor blockade with gabazine (right). Gabazine abolished the hyperpolarizing inhibitory component, resulting in large excitatory depolarizing responses. **(F)** Confocal images of DRN neurons filled with biocytin (red) during whole cell patch-clamp recordings and post hoc immuno-labelling for the serotonin marker tryptophane hydroxylase (TPH, blue). LH axon terminals are shown in yellow in the DRN expressing ChR2-eYFP. **(G)** Schematic of connectivity between LH and DRN. Paired Wilcoxon test. ** $p < 0.01$, *** $p < 0.001$.

Figure 5-source data 1. fig5_ephs.xlsx contains EPSC and IPSC amplitudes; related to figure 5.

Figure 5-source data 2. Fig5_stats.ipynb contains statistical analysis related to figure 5.

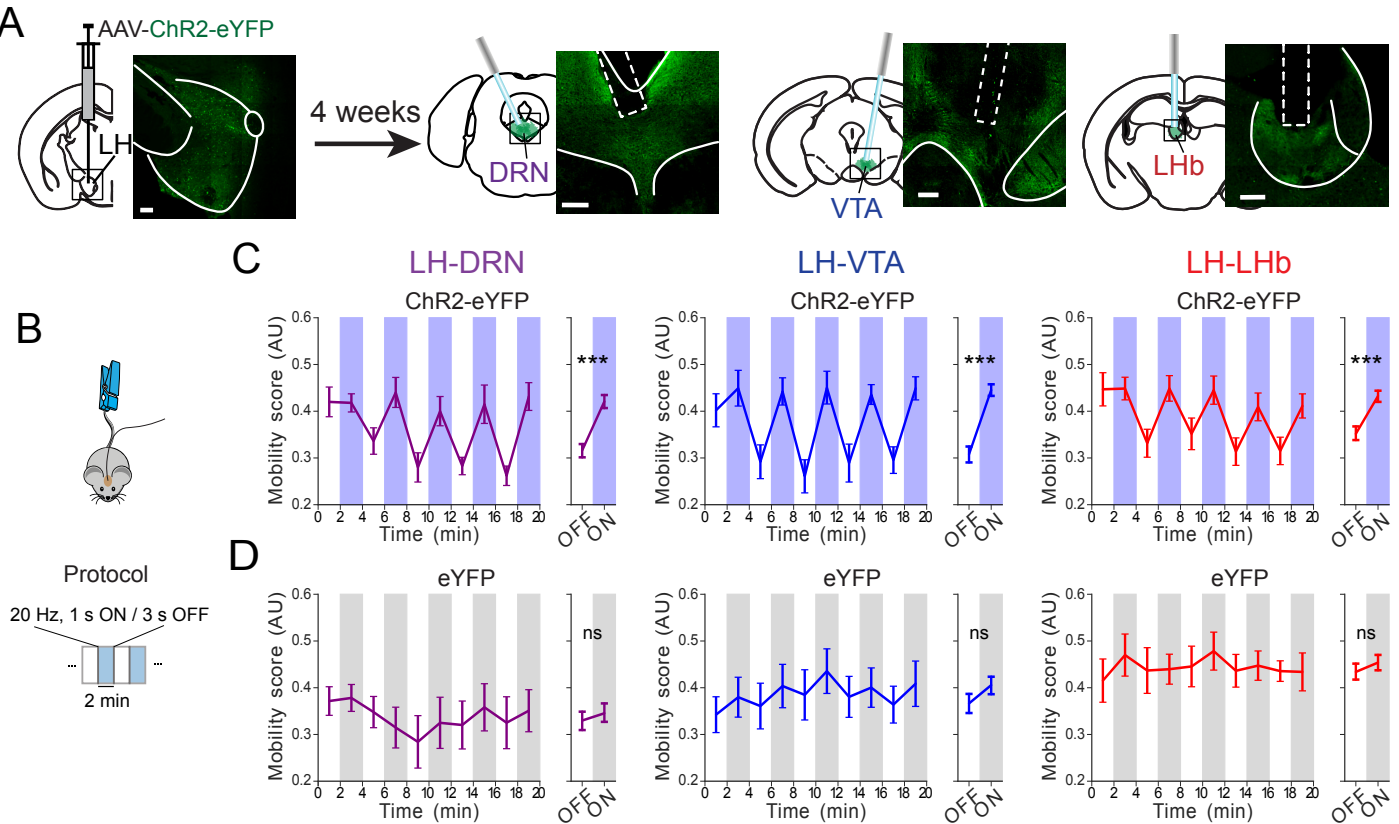


Figure 6. Optostimulation of the LH→DRN, LH→VTA, or LH→LHb pathway increases active coping behavior in the TST. **(A)** Diagram of the experimental setup and fluorescence images of ChR2-eYFP expression in LH neurons and axon terminals at the DRN, VTA, and LHb (scale bar 200 μ m). **(B)** Diagram of the experimental protocol for the TST. The mobility of the mice was evaluated during a 20 min TST session with alternating 2-min epochs without or with 1-s, 20 Hz trains every 4 sec. Mobility was automatically monitored with a video tracking system. **(C-D)** Plots of mean mobility (mean \pm SEM) during periods of optogenetic stimulation (blue **(C)** or gray **(D)**) or no light (white) at the LH→DRN (**left**), LH→VTA (**middle**), or LHA→LHb (**right**) pathways in ChR2-eYFP- **(C)** and eYFP-expressing **(D)** mice. Four-way repeated measures ANOVA between factors of group (ChR2-eYFP- and eYFP-expressing mice), and within factors pathway (LH→DRN, LH→VTA, or LH→LHb), time period (five 4-minutes periods) and laser (on and off) with post hoc Tukey test. The *p* values were adjusted using the Bonferroni multiple testing correction method. ****p* < 0.001, *p* > 0.2 ns (not significant).

Figure 6-Figure supplement 1. Optostimulation of the LH→DRN, LH→VTA, or LH→LHb pathway increases mobility in the OFT.

Figure 6-Figure supplement 2. Cannulae placement in mice expressing ChR2-eYFP

Figure 6-Figure supplement 3. Cannulae placement in mice expressing eYFP

Figure 6-source data 1. fig6_LHopto_TST-OFT.xlsx contains results of analysis of experiments in the TST and the OFT for mice expressing ChR2-eYFP and eYFP; related to figure 6 and figure supplement 1.

Figure 6-source data 2. Fig6_stats.ipynb contains statistical analysis related to figure 6.

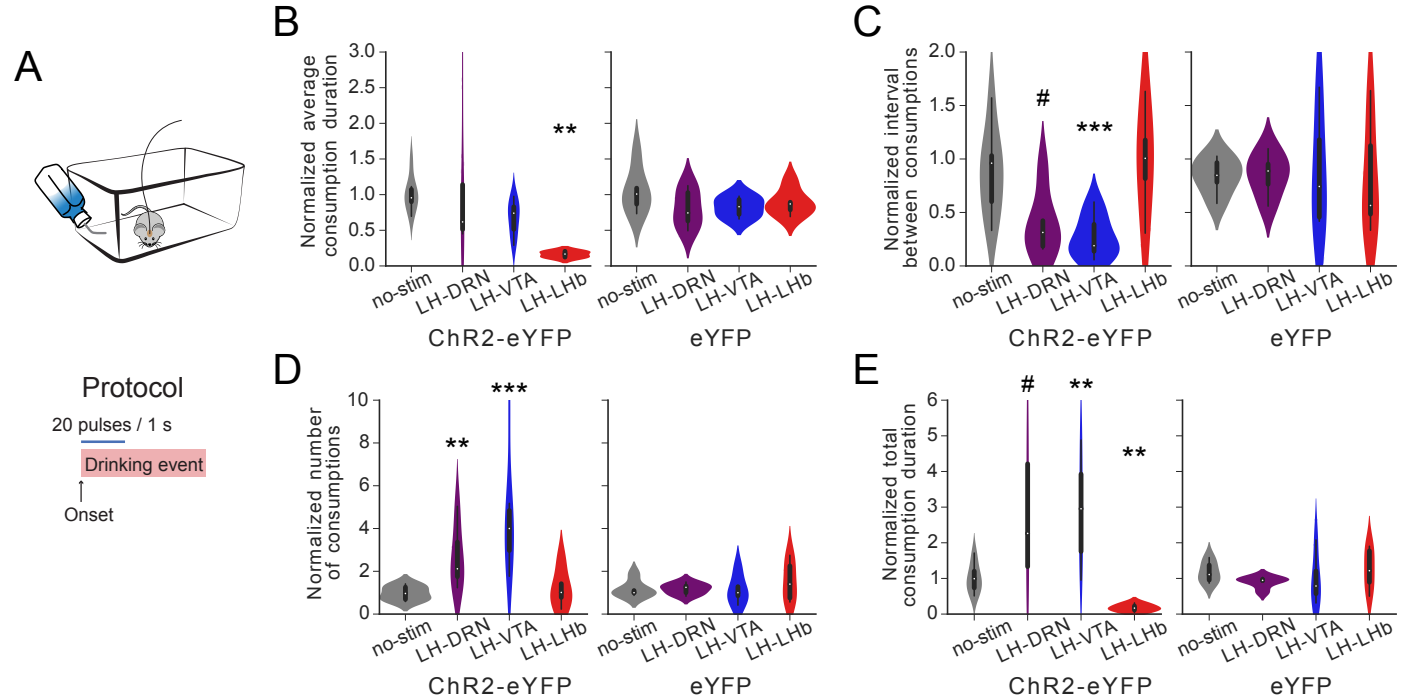


Figure 7. Optostimulation of LH neural outputs had distinct effects on sucrose consumption. **(A)** Diagram of the experimental protocol during sucrose consumption. A 1-s, 20 Hz optogenetic stimulation was given at the onset of a drinking event. **(B-E)** Plots of normalized average drinking duration (**B**), average interval between consumption events (**C**), total number of consumption events (**D**), and total drinking duration (**E**) normalized to a session without optogenetic stimulation for experimental mice expressing ChR2-eYFP (left panels) and control mice expressing eYFP only (right panels). Two-way ANOVA between factor of group (ChR2-eYFP- and eYFP-expressing mice) and within factor stimulated pathway (no stimulation, LH→DRN, LH→VTA, or LH→Lhb) with post hoc Dunnert's. The *p* values were adjusted using the Bonferroni multiple testing correction method. #*p* < 0.1, **p* < 0.05, ***p* < 0.01, ****p* < 0.001, *p* > 0.2 ns (not significant).

Figure 7-Figure supplement 1. Optostimulation of the LH→DRN, LH→VTA, or LH→Lhb pathways in the RTPP.

Figure 7-source data 1. fig7_LHopto_RTPP-SCT.xlsx contains results of analysis of experiments in the RTPP and the SCT for mice expressing ChR2-eYFP and eYFP; related to figure 7 and figure supplement 1.

Figure 7-source data 2. Fig7_stats.ipynb contains statistical analysis related to figure 7.

of LH neural outputs in reward-related behaviors, we examined the effect of optogenetic stimulation on sucrose consumption (**Figure 7**). To this end, water-deprived mice were allowed to drink the sucrose solution as described in the fiber photometry experiments, and 1-s, 20-Hz optogenetic stimulation were delivered at the onset of drinking events (**Figure 7A**). The effect of the optogenetic stimulation was compared to sessions without optogenetic manipulation (see Methods). The optogenetic stimulation of the LH→LHb pathway at the onset of drinking events decreased average drinking duration and total consumption, which is consistent with previous findings (**Stamatakis et al., 2016**). Conversely, optogenetic stimulation of the LH→VTA and LH→DRN pathways did not decrease drinking duration, but rather, decreased the time between drinking events, increased the total number of drinking events, and consequently increased total sucrose consumption (**Figure 7B-E**). Taken together, these results suggest that LH neural outputs use different mechanisms to control motivated behaviors.

Discussion

The LH is a central nucleus that connects many brain regions that orchestrates vital behaviours (**Bonnavion et al., 2016; Fakhoury et al., 2020**). It is the central brain region of an interconnected network that includes the DRN, VTA and the LHb, which all have important functions in reward and sensory processing, arousal, and motivation (**Bonnavion et al., 2016; Proulx et al., 2014; Nakamura, 2013; Morales and Margolis, 2017**). However, most studies have focused on distinct neurochemically defined LH populations or single downstream projections (**Bonnavion et al., 2016; Fakhoury et al., 2020; de Jong et al., 2019; Barbano et al., 2020; Lecca et al., 2020; Jennings et al., 2015; Lazaridis et al., 2019**). No studies have explored how multiple LH neural inputs or outputs are dynamically recruited in live animals performing behavioral tasks. Here, we examined how three major LH neural outputs are dynamically engaged in tasks involving cue processing and motivated behavioral responses. We used multi-fiber and dual-color photometry recordings to show that there is significant coherence in neural activity at LH neural outputs projecting to the DRN, VTA and LHb. These projections are from largely non-overlapping LH neuronal populations. Increased activity at these three pathways preceded mobility onset in the TST and preceded changes in the activity of serotonergic and dopaminergic neurons in the DRN and VTA, respectively. While the optogenetic stimulation of individual LH neural outputs was sufficient to increase the mobility of mice in the OFT and TST, it had a different effect on sucrose consumption. Optogenetic stimulation of the LH→LHb pathway reduced drinking duration and total sucrose consumption, whereas optogenetic stimulation of the LH→DRN and LH→VTA pathways decreased the interval between drinking events and, consequently increased the total number of drinking events and total sucrose consumption. These results indicates that these three LH neural outputs play complementary roles in engaging motivated behaviors.

Recent studies that measured neuronal activity in multiple brain regions have shown that coordinated neural network dynamics are important for organizing complex behaviors (**Allen et al., 2019; Steinmetz et al., 2019**). In line with these findings, our results provide evidence that three LH neural outputs act in concert to engage motivated behavioral responses. Our results support the role of LH as a central hub for signaling aversive cues to the DRN, the VTA, and the LHb in learned and innate defensive behaviors (**Barbano et al., 2020; de Jong et al., 2019; Trusel et al., 2019**). Moreover, we also demonstrate that all three LH neural outputs play an important role in initiating cue-independent spontaneously motivated active coping responses.

We combined retrograde tracing and intersectional viral approaches to show that only a few LH neurons project into two or more downstream brain regions. Our results further show that there are only a few collaterals, which is consistent with previous observations (**de Jong et al., 2019**). Our dual-color photometry recordings also confirmed that neural activity from two distinct LH neuronal populations projecting to DRN and VTA exhibit significant coherence. Taken together, these results are important for two reasons: (1) they show that independent LH neural populations

312 send coherent signals to downstream brain regions, and (2) they support the validity of recording
313 activity at axon terminals to study signal transmission along specific neural pathways.

314 The LHb receives a net excitatory input from the LH (*Lazaridis et al., 2019; Trusel et al., 2019*).
315 Recent work has shown that aversive stimuli are sufficient to activate the LH→LHb pathway and
316 promote escape behavior (*Lecca et al., 2017*). Moreover, this pathway encodes negative valences
317 and rapidly develops prediction signals for negative events and aversive cues, making this pathway
318 a critical node for value processing and avoidance learning (*Lazaridis et al., 2019; Trusel et al.,
319 2019*). The results we obtained in our active avoidance task are consistent with these findings.

320 The VTA receives both excitatory and inhibitory inputs from the LH, both of which play roles
321 in motivated behaviors (*Nieh et al., 2015, 2016; Barbano et al., 2016, 2020; de Jong et al., 2019*).
322 Glutamatergic transmission at the LH→VTA pathway (LH^{Glut} →VTA) plays a role in motivating innate
323 escape responses, signaling unexpected aversive outcomes, and signaling cues predicting aversive
324 outcomes (*de Jong et al., 2019; Barbano et al., 2020*). This aversive signal is mediated by the acti-
325 vation of VTA dopaminergic neurons projecting to the ventromedial section of the nucleus accum-
326 bens (*de Jong et al., 2019*). *Barbano et al. (2020)* showed that LH^{Glut} →VTA transmission mediates
327 innate escape responses by the activation of VTA glutamatergic neurons. GABAergic transmission
328 at the LH→VTA pathway (LH^{GABA} →VTA) plays an important role in promoting behavioral activation
329 leading to compulsive sucrose-seeking and feeding (*Nieh et al., 2015; Barbano et al., 2016*), behav-
330 iors that are mediated by the disinhibition of VTA dopamine neurons (*Nieh et al., 2015*). In light of
331 these findings, it is likely that the increased activity observed in aversive contexts (AP, TST, active
332 avoidance) is mediated by the LH^{Glut} →VTA transmission while the increased in activity measured
333 prior to sucrose consumption is mediated by the LH^{GABA} →VTA transmission. Taken together, these
334 results suggest that behavioral responses are engaged by an increase in the activity of DA neurons
335 in the VTA through direct activation (aversive contexts) or disinhibition (reward-seeking behavior)
336 of DA activity that originates from LH projections.

337 We show that the LH→DRN pathway is also involved in engaging motivated behavioral responses
338 in freely behaving mice. Serotonergic DRN neurons play important roles in organizing motivated
339 and reward-related behaviors (*Nakamura, 2013*), in emotions and aversive processing (*Cools et al.,
340 2008*), and in active coping behaviors (*Nishitani et al., 2019; Cools et al., 2008; Nakamura, 2013*).
341 Here we show that the LH→DRN pathway is activated when mice are presented with an aversive
342 airpuff or a mild foot shock. This pathway is also prominently engaged before the mice reach the
343 reward spout, as we observed with the LH→VTA pathway and at mobility onset, which indicates
344 that there is a significant correlation with mobility in the TST.

345 Both DRN^{5HT} and VTA^{DA} neurons increased their activity at the onset of mobility in coping be-
346 haviors such as the TST. This change in activity was preceded by the activation of the LH→DRN and
347 LH→VTA pathways, suggesting that signal transmission from the LH leads to the activation of the
348 DRN^{5HT} and VTA^{DA} neurons in order to control motivated responses.

349 In the DRN, serotonergic and GABAergic neurons receive prominent inputs from the LH (*Ogawa
350 and Watabe-Uchida, 2018; Weissbourd et al., 2014; Pollak Dorocic et al., 2014; Celada et al., 2002*).
351 *Zhou et al. (2017)* recently shown that functional excitatory and inhibitory inputs converge onto
352 serotonergic DRN neurons. Our *ex vivo* electrophysiological recordings showed similar inputs
353 converging onto non-serotonergic DRN neurons indicating that there is a complex functional
354 relationship between the LH and the DRN (*Celada et al., 2002*). However, it remains to be deter-
355 mined whether this increase in serotonergic activity is mediated by direct activation of 5-HT DRN
356 neurons or by indirect disinhibition through local GABAergic neurons.

357 We also show that all three LH neural outputs are activated prior to the onset of movement in
358 the TST, an energetically-demanding and aversive context (*Proulx et al., 2014; Warden et al., 2012*).
359 Recent miniscopic *in vivo* calcium imaging of LHb neurons in mice responding in looming experi-
360 ments has revealed that specific LHb neuron ensembles are active before the mice start running
361 away from an aversive threat (*Lecca et al., 2020*). Our results suggest that some of the excitatory
362 inputs driving these neuronal ensembles may be provided by the LH. Our results are also remi-

363 niscent of recent studies that directly measured the activity of orexin-expressing LH neurons and
364 shown that this cell population is activated by aversive stimuli and stressors and is inhibited dur-
365 ing food consumption, which is independent of food taste and texture (**González et al., 2016a,b**).
366 Moreover, the same group recently showed that a large fraction of orexin-expressing LH is acti-
367 vated at the onset of the initiation of movement (**Karnani et al., 2020**). We propose that signal
368 transmission from this genetically-defined population in the LH play an important role in motivat-
369 ing the initiation of movement by processing reward and sensory information in the DRN, VTA, and
370 LHb (**Flanigan et al., 2020; Harris et al., 2005**). Since most orexin-expressing neurons in the LH co-
371 release glutamate (**Rosin et al., 2003; Mickelsen et al., 2019**), it would be interesting to determine
372 how excitatory and orexigenic transmissions drive activity in the DRN, VTA, and LHb and as a result,
373 control motivated behaviors.

374 In the SCT, there was also a significant increase in the activity at the LH→DRN and LH→VTA path-
375 ways prior to the mice reaching the sucrose dispenser, while no significant change in the activity
376 at the LH→LHb pathway was observed in this task. These results suggest that the LH→DRN and
377 LH→VTA pathways may play a more general role in motivating goal-directed behavior, while the
378 LH→LHb pathway would be critically involved in orchestrating behavioral responses in aversive con-
379 texts. This notion is supported by previous experiments showing that the inhibition of the LH→LHb
380 pathway impaired aversion-driven escape behavior (**Lecca et al., 2017**) and disrupted avoidance
381 learning. The inhibition of the LH→VTA pathway also impaired innate defensive behavior (**Barbano
382 et al., 2020**). Our optogenetic experiments also support this scenario. Although the optogenetic
383 stimulation of individual LH neural outputs increased mobility in the TST, optogenetic stimulation
384 at drinking onset in the SCT had a different effect. Indeed, the activation of the LH→LHb path-
385 way at drinking onset decreased drinking duration and total sucrose consumption, whereas the
386 activation of the LH→DRN or the LH→VTA pathway increased total sucrose consumption by de-
387 creasing the time interval between drinking periods. One possible underlying mechanism that
388 enhances sucrose consumption following LH→VTA activation may be mediated by the co-release
389 of neuropeptides from LH axon terminals in the VTA, a neuropeptide that promotes reward-seeking
390 by enhancing glutamate transmission in the VTA (**Kempadoo et al., 2013**). In the SCT, phasic activity
391 at the LH^{GABA}→VTA pathway at the onset of sucrose consumption may also be sufficient to moti-
392 vate reward-seeking behaviors by decreasing time the interval between drinking periods (**Barbano
393 et al., 2016; Jennings et al., 2015**).

394 In summary, we show the LH→LHb, LH→VTA, and the LH→DRN pathways are important in
395 active coping and defensive behaviours. For many contexts and stimuli, the responses of the
396 LH→DRN, LH→VTA, and LH→LHb pathways are coherent, suggesting that the LH conveys com-
397 plementary information that engages several downstream brain regions to elicit motivated be-
398 haviors. It is likely that distinct 5-HT DRN, and DA VTA neuronal populations, segregated by their
399 inputs and outputs, play different but complementary roles in cue processing and adaptive behav-
400 iors. Another interesting question that remains to be investigated is whether the three distinct LH
401 neuronal populations, independently projecting to DRN, VTA and LHb, receive common or distinct
402 inputs from upstream brain regions.

403 Methods and Materials

404 Animals

405 All experiments were performed with 8- to 12-week-old wild-type C57BL/6J, ePet-cre, or DAT-ires-
406 cre mice. The mice were housed 2-4 per cage and were kept on a 12 h/12 h light/dark cycle. All
407 the experiments were performed in accordance with the Canadian Guide for the Care and Use
408 of Laboratory Animals guidelines and were approved by the Université Laval Animal Protection
409 Committee.

410 Stereotactic injections

411 The mice were anesthetized with isoflurane for the stereotaxic injections of adeno-associated viruses
412 (AAVs) and the implantation of optical fibers. Viral titers ranged from 10^{12} to 10^{13} genome copies per
413 milliliter and volumes ranged from 100 to 200 nl per side. Injections were performed using a glass
414 pipette mounted on a stereotactic table. The AAVs were infused at a rate of 1 nl/sec. At the end
415 of the injection, the pipet was left *in situ* for 5 min to allow the virus to diffuse into the surround-
416 ing tissue. Three to four weeks later, for the fiber photometry and optogenetic experiments, the
417 mice were implanted with 200- or 400 μm cannulae with a metal ferrule for the fiber photometry
418 recordings, and 200 μm cannulae with a ceramic ferrule for the optogenetic manipulations.

419 For most fiber photometry experiments, the mice were bilaterally injected with AAVDJ-CAG-
420 GCaMP6s in the LH, and optical fiber cannulae were implanted with their tips immediately above
421 the DRN, VTA, and Lhb. For the intersectional viral strategy, the mice were injected with retroAAV-
422 CAG-cre-P2A-mNeptune in the VTA, retroAAV-CAG-flpO-P2A-TagBFP2 in the DRN, and a mix of the
423 AAV9-CAG-DIO-jrGECO and AAV9-EF1a-fDIO-GCaMP6s in the LH, and an optocal fiber was chrono-
424 cally implanted above the LH. For the dual-color fiber photometry, ePet-cre mice were injected with
425 AAVDJ-CAG-GCaMP6s in the LH and AAV9-CAG-DIO-jrGECO1a in the DRN, and optical fiber was im-
426 planted above the DRN. Similarly, DAT-ires-cre mice were injected with AAVDJ-CAG-GCaMP6s in the
427 LH and AAV9-CAG-DIO-jrGECO1a in the VTA, and optical fiber was implanted above the VTA.

428 For the optogenetic experiments, the mice were bilaterally injected with AAV9-hSyn-hChR2(H134R)-
429 eYFP or AAV9-hSyn-eYFP in the LH, and optical fibers were implanted above the DRN, VTA, and Lhb.
430 The mice were tested 2 weeks post-cannulae implantation to give them time to recover from the
431 surgical procedures.

432 For the electrophysiology experiments, the mice were injected with AAV9-hSyn-hChR2(H134R)-
433 eYFP in the LH. Acute brain slices were prepared 3 weeks later for whole-cell patch clamp record-
434 ings.

435 To label DRN-, VTA-, and Lhb-projecting neurons in the LH of the same animal, the mice were
436 injected with CTx488 (Alexa Fluor 488-conjugated cholera toxin subunit B), CTx594, and CTx647 in
437 the DRN, VTA, and Lhb, respectively. The mice were transcardially perfused 3 days later, and their
438 brains were processed for histology.

439 The coordinates for the injections were as follows: LH : -1.2 mm AP, ± 1.0 mm ML, -5.2 mm DV;
440 Lhb : -1.65 mm AP, ± 0.45 mm ML, -2.8 mm DV; VTA : -3.3 mm AP, ± 0.5 mm ML, -4.8 mm DV; DRN
441 : -4.65 mm AP, 0.0 mm ML, -3.2 mm DV. The coordinates for implantation were the following: LH :
442 -1.2 mm AP, -1.0 mm ML, -5.0 mm DV; Lhb : -1.65 mm AP, -0.45 mm ML, -2.4 mm DV; VTA : -3.3
443 mm AP, 1.0 mm ML, -4.4 mm DV $\angle 10^\circ$; DRN : -4.65 mm AP, -1.05 mm ML, -2.9 mm DV $\angle 20^\circ$.

444 Fiber photometry recordings

445 A custom-build (*Kim et al., 2016*) or a Neurophotometrics
446 (<https://neurophotometrics.com>) fiber photometry systems was used to record calcium signals.
447 Both systems had the same set of dichroic mirrors, filters, and LEDs. Light from 415-nm, 470-nm,
448 and 560-nm LEDs were bandpass filtered, collimated, reflected by dichroic mirrors, and focused by
449 a 20 \times objective (numerical aperture, NA 0.39). The light passed through a patch cord of three fibers,
450 that were connected to the implanted cannulae. The emitted fluorescence was collected by the
451 same fibers, filtered, and separated into red and green images, which were projected on a CMOS
452 camera sensor. The excitation power was adjusted so as to get 50 to 70 μW of each of the lights
453 at the tip of the patch cord. The custom-build system was controlled using LabJack and a custom-
454 written Matlab code. The Neurophotometrics system was run by Bonsai open source software.
455 For most of the experiments, light from 415-nm- and 470-nm LEDs was alternated such that the
456 camera captured fluorescent excitation light from either the 415-nm or 470-nm LED. The camera
457 captured images at 20 Hz. Signals from the two excitation wavelengths were sampled at 10 Hz.
458 For the experiments with the ePet-cre and DAT-ires-cre mice, the 560-nm LED was alternated with
459 the 470-nm LED. For the intersectional viral strategy experiments, all three (415-nm, 470-nm, and

460 560-nm) LEDs were alternated such that the camera captured one light at a time. See *Martianova*
461 *et al.* (2019) for more details.

462 The mice were connected to a 3-fiber patch cord to record the signals during all the tests. For
463 intersectional viral strategy experiments with the ePet-cre and DAT-ires-cre mice, only one fiber
464 was connected.

465 **Airpuff test.**

466 The mice were placed in the open field arena and airpuffs were delivered on top of the animals
467 every 60 s, for a total of 5 airpuffs per 6 min session. Airpuff delivery was paired with a key press
468 on a computer keyboard that was registered by the fiber photometry software and that provided
469 timestamps of the airpuffs.

470 **Sucrose consumption test.**

471 The mice were water-deprived for 24 h before the experiment. For the test, the mice were placed
472 in a cage with free access to a spout delivering a small amount of sucrose solution. Consumption
473 periods were automatically tracked with a custom lickometer. The setup to measure licks con-
474 sisted of a mouse cage covered with a metal grid floor. The cage was equipped with a copper
475 wire-wrapped metal sipper tube from which sucrose solution was delivered. Each lick closed an
476 electrical circuit for the duration of the contact with the sipper tube. The junction potential be-
477 tween the metal sipper tube and the mouse was recorded using the ANY-maze system. ANY-maze
478 provided timestamps of each of the loop closures. To align the lick timestamps with the fiber pho-
479 tometry recordings, the start of the ANY-maze test was either triggered by the fiber photometry
480 system or by ANY-maze, and the fiber photometry software recorded the actual timestamps of the
481 same computer.

482 **Tail suspension test.**

483 The mice were suspended by their tail for 10 min. Movement was monitored using a camera and
484 ANY-maze video-tracking software. ANY-maze detects the speed of animal movement. The ANY-
485 maze recordings were aligned to the fiber photometry recordings using the same strategy as with
486 the sucrose consumption test.

487 **Open field test.**

488 The mice were placed in an open field (50 cm x 50 cm) and movement was tracked using a camera
489 and ANY-maze video-tracking software as with to the tail-suspension test.

490 **Avoidance Test.**

491 A mouse was placed in a two-compartment chamber (Med Associates). A conditioned stimulus (CS),
492 light, and tone was provided for 8 s pseudo-randomly with an average ITI of 40 s. At the end of the
493 8-s CS, a mild foot-shock (0.2–0.4 mA) was delivered through the grid floor for 8 s or until the mouse
494 crossed to the other compartment, which stopped the shock. If the mouse crossed within the 8-s
495 CS, no shock was delivered. This was referred as avoidance. The mice were tracked using a camera
496 and ANY-maze video-tracking software. To align the recordings of all the setups, Med Associates
497 software triggered the start of the fiber photometry and the ANY-maze software at the beginning
498 of the tests. The position of the mouse was analyzed post hoc using DeepLabCut, a toolbox for
499 markerless animal pose estimation. (*Mathis et al., 2018*).

500 **Optogenetic manipulations**

501 For the optogenetic experiments, the mice were connected to a 450-nm laser (Doric Lenses) through
502 an optical fiber and a rotary joint. Pulses of blue light were controlled by the ANY-maze software.
503 The stimulation protocol was 20-Hz trains and 5-ms pulses for 1 s every 4 s. The light intensity was
504 adjusted to provide 10 mW at the tips of the implanted optical fiber cannulae. During a trial, the

505 mice were connected to a single optical fiber cannula implanted above the DRN, VTA, or LHb. For
506 each test, the mice were tested on consecutive days using a Latin square experimental design.

507 **Real-time place preference test.**

508 The mice were placed in a chamber with two compartments connected by a small corridor. After
509 1 min of habituation, one of the compartments was paired with an optogenetic stimulation. A
510 mouse received a photostimulation every time it entered the paired chamber (randomly assigned).
511 To maximize novelty and exploratory behavior on consecutive testing days, the RTPP apparatus
512 was used as follows: day 1 with a plain floor, day 2 with bedding covering the floor, and day three
513 with finely ground food pellet on the floor. Stimulation chambers were randomly assigned on each
514 of the three days of testing. The location of the mouse (chamber 1, chamber 2, or corridor) was
515 tracked, and laser activation was controlled using the ANY-maze video-tracking system.

516 **Tail suspension test and open field test.**

517 The mice were suspended by their tail for 20 min. The photostimulation was alternated between
518 a 2-min periods without stimulation and with a 2-min period with photostimulation trains (20 Hz,
519 1 second, 5-ms pulse duration, every 4 seconds).

520 **Sucrose consumption test.**

521 The same protocol used for the fiber photometry recordings was used for the optogenetic ma-
522 nipulations. The ANY-maze tracking system detected drinking onset and triggered 1-s 20-Hz laser
523 photostimulations for each drinking event. To define the baseline of drinking behavior for each
524 animal, the mice were tested 3 times (without photostimulation) prior to the photostimulation
525 sessions, and 1 time after (without photostimulation). The DRN, VTA, and LHb photostimulation
526 sessions and the sessions with no photostimulation were alternated using a Latin square experi-
527 mental design.

528 **Electrophysiology**

529 Three weeks after the injection of AAV-ChR2-eYFP in the LH, the mice were anesthetized with isoflu-
530 rane and were perfused transcardially with 10 mL of ice-cold NMDG-artificial cerebrospinal fluid
531 (aCSF) solution containing (in mM): 1.25 NaH₂PO₄, 2.5 KCl, 10 MgCl₂, 20 HEPES, 0.5 CaCl₂, 24
532 NaHCO₃, 8 D-glucose, 5 L-ascorbate, 3 Na-pyruvate, 2 thiourea, and 93 NMDG (osmolarity was ad-
533 justed to 300–310 mOsmol/L with sucrose). The pH was adjusted to 7.4 using 10 N HCl. Kynurenic
534 acid (2 mM) was added to the perfusion solution on the day of the experiment. The brains were
535 then quickly removed, and 250 μ m acute brain slices encompassing the DRN were prepared us-
536 ing a Leica VT1200S vibratome. The slices were placed in a 32°C oxygenated perfusion solution
537 for 10 min and were then incubated for 1 h at room temperature in HEPES-aCSF solution (in mM):
538 1.25 NaH₂PO₄, 2.5 KCl, 10 MgCl₂, 20 HEPES, 0.5 CaCl₂, 24 NaHCO₃, 2.5 D-glucose, 5 L-ascorbate, 1
539 Na-pyruvate, 2 thiourea, 92 NaCl, and 20 sucrose (osmolarity was adjusted to 300–310 mOsmol/L
540 with sucrose). The pH was adjusted to 7.4 using 10 N HCl. They were then transferred to a record-
541 ing chamber on the stage of an upright microscope (Zeiss) where they were perfused with 3–4
542 mL/min of aCSF (in mM): 120 NaCl, 5 HEPES, 2.5 KCl, 1.2 NaH₂PO₄, 2 MgCl₂, 2 CaCl₂, 2.5 glucose,
543 24 NaHCO₃, and 7.5 sucrose). The perfusion chamber and the aCSF were kept at 32°C. All the
544 solutions were oxygenated with 95% O₂/5% CO₂. A 60x water immersion objective and a video
545 camera (Zeiss) were used to visualize neurons in the DRN. Borosilicate glass (3–7 M Ω resistance)
546 recording pipettes were pulled using a P-1000 Flaming/ Brown micropipette puller (Sutter Instru-
547 ments). Recordings were performed using an Axopatch 200B amplifier (Molecular Devices). For the
548 voltage-clamp recordings, the intracellular solution consisted of (in mM): 115 cesium methanesul-
549 fonate, 20 cesium chloride, 10 HEPES, 2.5 MgCl₂, 4 Na₂ATP, 0.4 Na₃GTP, 10 Na-phosphocreatine,
550 0.6 EGTA, and 5 QX314, as well as 0.2% biocytin (pH 7.35). For the current-clamp recordings, the
551 intracellular solution consisted of (in mM): 130 K-gluconate, 5 KCl, 10 HEPES, 2.5 MgCl₂, 4 Na₂ATP,

552 0.4 Na3GTP, 10 Na-phosphocreatine, and 0.6 EGTA (pH 7.35). Signals were filtered at 5 kHz using
553 a Digidata 1500A data acquisition interface (Molecular Devices, San Jose, CA) and acquired using
554 pClamp 10.6 software (Molecular Devices). Pipette and cell capacitance were fully compensated.
555 To examine monosynaptic transmission, the extracellular recording solution was supplemented
556 with 1 μ M TTX and 100 μ M 4-AP. For the voltage-clamp experiments, postsynaptic currents were
557 measured in DRN neurons clamped at -60 mV and 0 mV holding voltage following optogenetic
558 stimulation of LH axon terminals with 5-ms blue light pulses delivered through the objective with
559 a Colibri 7 LED light source (Zeiss). Excitatory and inhibitory transmissions were blocked with 3
560 mM NBQX and 10 mM gabazine, which are AMPA and GABA-a receptor antagonists, respectively.
561 For the current-clamp experiments, DRN neurons were depolarized at -30mV and changes in the
562 postsynaptic potential were measured before and after the addition of 10 mM gabazine. Once the
563 recordings were completed, the slices were fixed in 4% formaldehyde for 30 min and were then
564 transferred to a 0.1M phosphate buffer solution for post hoc histological analysis.

565 **Histology and immunostaining**

566 The mice were deeply anesthetized using a mix of ketamine/xylazine (100 and 10 mg/kg, respec-
567 tively, intraperitoneally) and were transcardially perfused with saline followed by a 0.1 M phos-
568 phate buffer solution (PB, pH7.4) containing 4% paraformaldehyde. The brains were postfixed
569 overnight in the same solution, rinsed with PB, and stored in PB. Brain sections (100 μ m for histol-
570 ogy and 50 μ m for immunostaining) were cut with a vibratome along the coronal plane.

571 Sections used for fiber photometry recordings and optogenetic manipulations were examined
572 to confirm injection sites and cannulae placements. Recordings were excluded post hoc in the rare
573 cases where an optical fiber was misplaced or where the expression of the construct of interest
574 was off-target or low.

575 DRN sections from ePet-cre mice and VTA sections from DAT-ires-cre mice were stained for TPH
576 (tryptophan hydroxylase, a marker for 5HT neurons) and for TH (tyrosine hydroxylase, a marker for
577 DA neurons), respectively, using a standard 2-day immunostaining protocol. Briefly, free-floating
578 slices were first blocked in PB containing 10% normal donkey serum (NDS) and 0.2% Triton X-100
579 for 1 h. They were then incubated overnight with primary antibodies diluted in PB containing 3%
580 NDS and 0.2% Triton X-100 and then with a secondary antibody diluted in PB containing 3% NDS
581 for 2 h at RT. The primary antibodies were anti-TPH (Millipore, sheep polyclonal, 1:1000 dilution)
582 and anti-TH (Millipore, sheep polyclonal, 1:1000 dilution). The secondary antibody was donkey
583 anti-sheep IgG DyLight™ 405 (Jackson ImmunoResearch, 1:500 dilution).

584 Sections from the electrophysiological recordings were immunostained for TPH using the pro-
585 tocol described above. Immunostained sections and sections from mice injected with CTx were
586 mounted using Fluoromount™ Aqueous Mounting Medium (Millipore-Sigma) and imaged using a
587 Zeiss LSM700 confocal microscope.

588 **Data analysis**

589 Fiber photometry data.

590 To store, process, analyze, and visualize the fiber photometry data, a Python package of objects
591 and functions was created, which is available at [Fiber Photometry Data Analysis](#) GitHub repository.

592 To calculate the standardized dF/F (*z-score* dF/F , zdF/F), the algorithm described in [Mar-](#)
593 [tianova et al. \(2019\)](#) was used. Briefly, calcium-dependent (*signals*) and calcium-independent (*references*)
594 traces were smoothed using a band-pass filter (moving average was used in [Martianova et al.](#)
595 [\(2019\)](#)), flattened by removing the baseline using an airPLS algorithm (adaptive iteratively reweighted
596 Penalized Least Squares ([Zhang et al., 2010](#))), and standardized to a mean value of 0 and a stan-
597 dard deviation of 1. *References* were fitted to *signals* using a non-negative robust least squares
598 regression (Lasso algorithm), and zdF/F was calculated by subtraction from standardized *signals*
599 standardized and fitted *references*.

600 To define the onsets and offsets of consumption, lickings recorded with the lickometer were
601 used: onsets were defined as licks that persisted for at least 0.5 s, and offsets defined as the ab-
602 sence of licks for at least 1 s.

603 For most of the tests, ANY-maze provided the speed of the mice over time. For the avoidance
604 conditioning test, the coordinates of the mice over time were exported from videos using the
605 DeepLabCut toolbox (*Mathis et al., 2018*), and the speed was calculated using the following for-
606 mula: $(speed = \frac{\sqrt{(x_1-x_0)^2+(y_1-y_0)^2}}{(t_1-t_0)})$. To account for different tracking setups and experimental setups,
607 all the speeds were transformed to a standardized range [0, 1] (mobility score).

608 A mobility score was used to define mobility and immobility onsets. An immobility bout was
609 defined as a period where the values were < 0.1 and lasted at least 2 s.

610 zdF/F was aligned and averaged around the specific events such as airpuff, consumption onset,
611 mobility onset, CS, across all trials for each animal. To measure the change from a baseline area
612 under the curve (AUC) was calculated. For airpuff, baseline AUC was calculated at -2 – -1 s, airpuff
613 - at 0 – 1.5 s. For consumption onset, baseline AUC was calculated at -2 – -1 s, onset – at -0.5 – 1 s,
614 drinking – at 2 – 4 s. For immobility onset, immobile AUC was calculated at -3 – -1 s, pre-onset – at
615 -1 – 0 s, onset – at 0 – 1 s, mobile – at 1 – 3 s. In avoidance test, baseline AUC was calculated at -2 –
616 -1 s, CS – at 0 – 8 s, crossed – at 8 – 11 s. AUC was normalized to the duration of the area.

617 Optogenetics data.

618 For the RTPP, ANY-maze data of laser activity over time was exported from ANY-maze and the
619 preference score was calculated using the following formula: $preferencescore = \frac{time_{laserON} - time_{laserOFF}}{total\ time}$
620 as detailed before (*Proulx et al., 2018*).

621 For the OFT and TST, the speeds tracked by ANY-maze were transformed into a standardized
622 range [0, 1] (mobility score) to maintain the same format as the fiber photometry data. Average
623 mobility scores were calculated for periods of laser ON and OFF.

624 For the SCT, ANY-maze data of licks recorded over time were exported, and the consumption
625 onsets and offsets were found as described above. The following parameters were calculated:
626 average consumption duration, average interval between events, number of events, and total con-
627 sumption duration for three pre-sessions without photostimulation, sessions with photostimula-
628 tion, and one post-session without stimulation. As the last pre-session and the post-session had
629 approximately the same values for the parameters measured, these values were averaged and
630 were used for the data normalization of values acquired during sessions with photostimulation.

631 Statistical analyses.

632 Statistical analyses were performed using R programming language. Data distributions were tested
633 using the Shapiro-Wilk normality test. Parametric or nonparametric tests were chosen depending
634 on the number of observations, the distribution, and the model. For most of the data, a multi-factor
635 mixed ANOVA with post hoc Dunnett's or Tukey tests was used . The exact tests are indicated in
636 the figure legends and ipynb source data files. Significance was set at p<0.05 in most tests. Elec-
637 trophysiological and behavior experiments were replicated at least three times. Sample size were
638 estimated from previously published work and from pilot experiments performed in our labora-
639 tory.

640 Data and code availability

641 Raw data and the analysis steps from all the fiber photometry recordings and optogenetics manip-
642 ulations were saved in hierarchical data format (h5) files. A Python code with the classes, functions,
643 and an example of steps of analysis, including statistical analysis, was saved in Jupyter notebooks
644 and is available at the following GitHub repository: [Fiber Photometry Data Analysis](#)

645 Acknowledgments

646 We would like to thank Drs Armen Saghatelyan, Martin Lévesque, Sage Aronson and Sadegh Nabavi
647 for their critical reviews of the manuscript. We also thank the Plateforme d'Outils Moléculaires at
648 the CERVO Brain Center for producing the viral vectors, and Martin Lévesque's lab for providing the
649 DAT-ires-cre mice. CDP is supported by the Canadian Institutes of Health Research grant PJT169117
650 and the Natural Science and Engineering Research Council of Canada grant RGPIN-2017-06131, and
651 receives Fonds de Recherche en Santé du Québec (FRQS) Junior-1 salary support. EM is supported
652 by a doctoral training scholarship from the FRQS.

653 References

- 654 Allen WE, Chen MZ, Pichamoorthy N, Tien RH, Pachitariu M, Luo L, Deisseroth K. Thirst regulates moti-
655 vated behavior through modulation of brainwide neural population dynamics. *Science* (New York, NY).
656 2019; 364(6437):253. <http://www.ncbi.nlm.nih.gov/pubmed/30948440>
657 <http://www.ncbi.nlm.nih.gov/pmc/articles/PMC6711472/>, doi: 10.1126/science.aav3932.
- 658 Amat J, Sparks PD, Matus-Amat P, Griggs J, Watkins LR, Maier SF. The role of the habenular complex in the
659 elevation of dorsal raphe nucleus serotonin and the changes in the behavioral responses produced by un-
660 controllable stress. *Brain research*. 2001 oct; 917(1):118–26. <http://www.ncbi.nlm.nih.gov/pubmed/11602236>,
661 doi: 10.1016/s0006-8993(01)02934-1.
- 662 Bäckman CM, Malik N, Zhang Y, Shan L, Grinberg A, Hoffer BJ, Westphal H, Tomac AC. Characterization of a
663 mouse strain expressing Cre recombinase from the 3' untranslated region of the dopamine transporter locus.
664 *Genesis* (New York, NY : 2000). 2006 aug; 44(8):383–90. <http://www.ncbi.nlm.nih.gov/pubmed/17549727>
665 <http://www.ncbi.nlm.nih.gov/pmc/articles/PMC2668205/>
666 <http://doi.wiley.com/10.1002/dvg.20286>
667 <http://www.ncbi.nlm.nih.gov/pubmed/6865686>
668 <http://www.ncbi.nlm.nih.gov/pmc/articles/PMC16865686/>, doi: 10.1002/dvg.20228.
- 669 Barbano MF, Wang HL, Morales M, Wise RA. Feeding and Reward Are Differentially Induced by Activating
670 GABAergic Lateral Hypothalamic Projections to VTA. *The Journal of neuroscience : the official journal of the*
671 *Society for Neuroscience*. 2016 mar; 36(10):2975–85. <http://www.ncbi.nlm.nih.gov/pubmed/26961951>
672 <http://www.ncbi.nlm.nih.gov/pmc/articles/PMC4783499/>, doi: 10.1523/JNEUROSCI.3799-15.2016.
- 673 Barbano MF, Wang HL, Zhang S, Miranda-Barrientos J, Estrin DJ, Figueroa-González A, Liu B, Barker DJ,
674 Morales M. VTA Glutamatergic Neurons Mediate Innate Defensive Behaviors. *Neuron*. 2020 jul; 107(2):368–
675 382.e8. <http://www.ncbi.nlm.nih.gov/pubmed/32442399>
676 <http://www.ncbi.nlm.nih.gov/pmc/articles/PMC7381361/>, doi: 10.1016/j.neuron.2020.04.024.
- 677 Bonnavion P, Mickelsen LE, Fujita A, de Lecea L, Jackson AC. Hubs and spokes of the lateral hypothalamus: cell
678 types, circuits and behaviour. *Journal of Physiology*. 2016; 594(22):6443–6462. doi: 10.1113/jp271946.
- 679 Celada P, Casanova JM, Paez X, Artigas F. Control of serotonergic neurons in the dorsal raphe nucleus by the
680 lateral hypothalamus. *Brain research*. 2002 apr; 932(1-2):79–90. <http://www.elsevier.com/locate/bres>
681 <http://www.ncbi.nlm.nih.gov/pubmed/11911864>, doi: 10.1016/s0006-8993(02)02284-9.
- 682 Commons KG, Cholanians AB, Babb JA, Ehlinger DG. The Rodent Forced Swim Test Measures Stress-
683 Coping Strategy, Not Depression-like Behavior. *ACS chemical neuroscience*. 2017 may; 8(5):955–
684 960. <http://www.ncbi.nlm.nih.gov/pubmed/28287253>
685 <http://www.ncbi.nlm.nih.gov/pmc/articles/PMC5518600/>, doi: 10.1021/acscchemneuro.7b00042.
- 686 Cools R, Roberts AC, Robbins TW. Serotoninergic regulation of emotional and behavioural control processes.
687 *Trends in Cognitive Sciences*. 2008; 12(1):31–40. doi: 10.1016/j.tics.2007.10.011.
- 688 Dana H, Mohar B, Sun Y, Narayan S, Gordus A, Hasseman JP, Tsegaye G, Holt GT, Hu A, Walpita D, Patel R,
689 Macklin JJ, Bargmann CI, Ahrens MB, Schreiter ER, Jayaraman V, Looger LL, Svoboda K, Kim DS. Sensitive
690 red protein calcium indicators for imaging neural activity. *eLife*. 2016; 5(MARCH2016). <http://www.ncbi.>
691 <http://www.ncbi.nlm.nih.gov/pubmed/27011354>
692 <http://www.ncbi.nlm.nih.gov/pmc/articles/PMC4846379/>, doi:
693 10.7554/eLife.12727.
- 694 Dolzani SD, Baratta MV, Amat J, Watkins LR, Maier SF, Agster KL, Saddoris MP. Activation of a Habenulo – Raphe
695 Circuit Is Critical for the Behavioral and Neurochemical Consequences of Uncontrollable Stress in the Male
696 Rat. *eNeuro*. 2016; 3(5):e0229–16. doi: 10.1523/ENEURO.0229-16.2016.

- Fakhoury M**, Salman I, Najjar W, Merhej G, Lawand N. The Lateral Hypothalamus: An Uncharted Territory for Processing Peripheral Neurogenic Inflammation. *Frontiers in neuroscience*. 2020 feb; 14(8):101. <https://www.frontiersin.org/article/10.3389/fnins.2020.00101/full><http://www.ncbi.nlm.nih.gov/pubmed/3211653><http://www.ncbi.nlm.nih.gov/pubmed/32116534><http://www.ncbi.nlm.nih.gov/pmc/articles/PMC7029733/>, doi: 10.3389/fnins.2020.00101.

Flanigan ME, Aleyasin H, Li L, Burnett CJ, Chan KL, LeClair KB, Lucas EK, Matikainen-Ankney B, Durand-de Cottoli R, Takahashi A, Menard C, Pfau ML, Golden SA, Bouchard S, Calipari ES, Nestler Ej, DiLeone RJ, Yamanaka A, Huntley GW, Clem RL, et al. Orexin signaling in GABAergic lateral habenula neurons modulates aggressive behavior in male mice. *Nature Neuroscience*. 2020 may; 23(5):638-650. <http://www.ncbi.nlm.nih.gov/pubmed/32284606><http://www.ncbi.nlm.nih.gov/pmc/articles/PMC7195257/>, doi: 10.1038/s41593-020-0617-7.

González JA, Iordanidou P, Strom M, Adamantidis A, Burdakov D. Awake dynamics and brain-wide direct inputs of hypothalamic MCH and orexin networks. *Nature Communications*. 2016 apr; 7:11395. <http://www.nature.com/doifinder/10.1038/ncomms11395>, doi: 10.1038/ncomms11395.

González JA, Jensen LT, Iordanidou P, Strom M, Fugger L, Burdakov D. Inhibitory Interplay between Orexin Neurons and Eating. *Current Biology*. 2016 sep; 26(18):2486-2491. <https://linkinghub.elsevier.com/retrieve/pii/S0960982216307643>, doi: 10.1016/j.cub.2016.07.013.

Harris GC, Wimmer M, Aston-Jones G. A role for lateral hypothalamic orexin neurons in reward seeking. *Nature*. 2005 sep; 437(7058):556-9. <http://www.nature.com/articles/nature04071><http://www.ncbi.nlm.nih.gov/pubmed/16100511>, doi: 10.1038/nature04071.

Hassani OK, Krause MR, Mainville L, Cordova CA, Jones BE. Orexin Neurons Respond Differentially to Auditory Cues Associated with Appetitive versus Aversive Outcomes. *Journal of Neuroscience*. 2016; 36(5):1747-1757. <http://www.jneurosci.org/cgi/doi/10.1523/JNEUROSCI.3903-15.2016>, doi: 10.1523/JNEUROSCI.3903-15.2016.

Jennings JH, Ung RL, Resendez SL, Stamatakis AM, Taylor JG, Huang J, Veleta K, Kantak PA, Aita M, Shilling-Scrivo K, Ramakrishnan C, Deisseroth K, Otte S, Stuber GD. Visualizing Hypothalamic Network Dynamics for Appetitive and Consummatory Behaviors. *Cell*. 2015 jan; 160(3):516-527. <http://dx.doi.org/10.1016/j.cell.2014.12.026><https://linkinghub.elsevier.com/retrieve/pii/S0092867414016328>, doi: 10.1016/j.cell.2014.12.026.

de Jong JW, Afjei SA, Pollak Dorocic I, Peck JR, Liu C, Kim CK, Tian L, Deisseroth K, Lammel S. A Neural Circuit Mechanism for Encoding Aversive Stimuli in the Mesolimbic Dopamine System. *Neuron*. 2019; 101(1):133-151.e7. <https://linkinghub.elsevier.com/retrieve/pii/S0896627318309966><http://www.ncbi.nlm.nih.gov/pubmed/30503173><http://www.ncbi.nlm.nih.gov/pmc/articles/PMC6317997/>, doi: 10.1016/j.neuron.2018.11.005.

Kakava-Georgiadou N, Zwartkruis MM, Bullich-Vilarrubias C, Luijendijk MCM, Garner KM, van der Plasse G, Adan RAH. An intersectional approach to target neural circuits with cell- and projection-type specificity: Validation in the mesolimbic dopamine system. *Frontiers in Molecular Neuroscience*. 2019; 12(February):1-9. doi: 10.3389/fnmol.2019.00049.

Karnani MM, Schöne C, Bracey EF, González JA, Viskaitis P, Li HT, Adamantidis A, Burdakov D. Role of spontaneous and sensory orexin network dynamics in rapid locomotion initiation. *Progress in neurobiology*. 2020 apr; 187:101771. <http://www.ncbi.nlm.nih.gov/pubmed/32058043><http://www.ncbi.nlm.nih.gov/pmc/articles/PMC7086232/>, doi: 10.1016/j.pneurobio.2020.101771.

Kempadoo KA, Tourino C, Cho SL, Magnani F, Leininger GM, Stuber GD, Zhang F, Myers MG, Deisseroth K, de Lecea L, Bonci A. Hypothalamic neuropeptides promote reward by enhancing glutamate transmission in the VTA. *The Journal of neuroscience : the official journal of the Society for Neuroscience*. 2013 may; 33(18):7618-26. <http://www.ncbi.nlm.nih.gov/pubmed/23637156><http://www.ncbi.nlm.nih.gov/pmc/articles/PMC3865559/>, doi: 10.1523/JNEUROSCI.2588-12.2013.

Kim CK, Yang SJ, Pichamoorthy N, Young NP, Kauvar I, Jennings JH, Lerner TN, Berndt A, Lee SY, Ramakrishnan C, Davidson TJ, Inoue M, Bito H, Deisseroth K. Simultaneous fast measurement of circuit dynamics at multiple sites across the mammalian brain. *Nature methods*. 2016 apr; 13(4):325-8. <http://www.ncbi.nlm.nih.gov/pubmed/26878381><http://www.ncbi.nlm.nih.gov/pmc/articles/PMC5717315/>, doi: 10.1038/nmeth.3770.

- 746 Lazaridis I, Tzortzi O, Weglage M, Märtin A, Xuan Y, Parent M, Johansson Y, Fuzik J, Fürth D, Fenno LE, Ramakr-
747 ishnan C, Silberberg G, Deisseroth K, Carlén M, Meletis K. A hypothalamus-habenula circuit controls aver-
748 sion. *Molecular psychiatry*. 2019 sep; 24(9):1351–1368. <http://www.ncbi.nlm.nih.gov/pubmed/30755721>
749 <http://www.ncbi.nlm.nih.gov/articlerender.fcgi?artid=PMC6756229>, doi: 10.1038/s41380-019-0369-5.
- 750 Lecca S, Meye FJ, Trusel M, Tchenio A, Harris J, Schwarz MK, Burdakov D, Georges F, Mameli M. Aversive
751 stimuli drive hypothalamus-to-habenula excitation to promote escape behavior. *eLife*. 2017 sep; 6(3):179–
752 82. <http://www.ncbi.nlm.nih.gov/pubmed/28871962>
753 <http://www.ncbi.nlm.nih.gov/articlerender.fcgi?artid=PMC5606847>
<http://www.ncbi.nlm.nih.gov/pubmed/12242150>, doi: 10.7554/eLife.30697.
- 754 Lecca S, Namboodiri VMK, Restivo L, Gervasi N, Pillolla G, Stuber GD, Mameli M. Heteroge-
755 neous Habenular Neuronal Ensembles during Selection of Defensive Behaviors. *Cell reports*. 2020
756 jun; 31(10):107752. <http://www.ncbi.nlm.nih.gov/pubmed/32521277>
757 <http://www.ncbi.nlm.nih.gov/articlerender.fcgi?artid=PMC7296347>, doi: 10.1016/j.celrep.2020.107752.
- 758 Martianova E, Aronson S, Proulx CD. Multi-Fiber Photometry to Record Neural Activity in Freely-Moving Ani-
759 mals. *Journal of visualized experiments : JoVE*. 2019 oct; 2019(152). <http://www.ncbi.nlm.nih.gov/pubmed/31680685>, doi: 10.3791/60278.
- 761 Mathis A, Mamidanna P, Cury KM, Abe T, Murthy VN, Mathis MW, Bethge M. DeepLabCut: markerless pose
762 estimation of user-defined body parts with deep learning. *Nature Neuroscience*. 2018; p. 1. <http://www.nature.com/articles/s41593-018-0209-y>, doi: 10.1038/s41593-018-0209-y.
- 764 Mickelsen LE, Bolisetty M, Chimileski BR, Fujita A, Beltrami Ej, Costanzo JT, Naparstek JR, Robson P, Jackson
765 AC. Single-cell transcriptomic analysis of the lateral hypothalamic area reveals molecularly distinct popula-
766 tions of inhibitory and excitatory neurons. *Nature neuroscience*. 2019 apr; 22(4):642–656. [http://www.ncbi.nlm.nih.gov/pubmed/30858605](http://www.ncbi.
767 nlm.nih.gov/pubmed/30858605)
768 <http://www.ncbi.nlm.nih.gov/articlerender.fcgi?artid=PMC7043322>, doi:
10.1038/s41593-019-0349-8.
- 769 Morales M, Margolis EB. Ventral tegmental area: cellular heterogeneity, connectivity and behaviour. *Nature*
770 reviews Neuroscience. 2017 feb; 18(2):73–85. <http://www.ncbi.nlm.nih.gov/pubmed/28053327>, doi:
771 10.1038/nrn.2016.165.
- 772 Nakamura K. The role of the dorsal raphe nucleus in reward-seeking behavior. *Frontiers in Integrative Neu-
773 roscience*. 2013; 7(August):1–18. <http://journal.frontiersin.org/article/10.3389/fnint.2013.00060/abstract>, doi:
774 10.3389/fnint.2013.00060.
- 775 Nieh EH, Matthews GA, Allsop SA, Presbrey KN, Leppla CA, Wichmann R, Neve R, Wildes CP, Tye KM. Decoding
776 neural circuits that control compulsive sucrose seeking. *Cell*. 2015 jan; 160(3):528–41. [http://dx.doi.org/10.1016/j.cell.2015.01.003](http://dx.doi.org/
777 10.1016/j.cell.2015.01.003)
778 <http://linkinghub.elsevier.com/retrieve/pii/S009286741500045>
779 <http://www.ncbi.nlm.nih.gov/pubmed/25635460>
<http://www.ncbi.nlm.nih.gov/articlerender.fcgi?artid=PMC4312417>, doi:
10.1016/j.cell.2015.01.003.
- 780 Nieh EH, Vander Weele CM, Matthews GA, Presbrey KN, Wichmann R, Leppla CA, Izadmehr EM, Tye KM. In-
781 hibitory Input from the Lateral Hypothalamus to the Ventral Tegmental Area Disinhibits Dopamine Neurons
782 and Promotes Behavioral Activation. *Neuron*. 2016; 90(6):1286–1298. <http://dx.doi.org/10.1016/j.neuron.2016.04.035>, doi: 10.1016/j.neuron.2016.04.035.
- 784 Nishitani N, Nagayasu K, Asaoka N, Yamashiro M, Andoh C, Nagai Y, Kinoshita H, Kawai H, Shibui N, Liu B, Hewin-
785 son J, Shirakawa H, Nakagawa T, Hashimoto H, Kasparov S, Kaneko S. Manipulation of dorsal raphe sero-
786 tonergic neurons modulates active coping to inescapable stress and anxiety-related behaviors in mice and
787 rats. *Neuropsychopharmacology : official publication of the American College of Neuropsychopharmacology*.
788 2019; 44(4):721–732. <http://dx.doi.org/10.1038/s41386-018-0254-y>
789 <http://www.ncbi.nlm.nih.gov/pubmed/30377380>
790 <http://www.ncbi.nlm.nih.gov/articlerender.fcgi?artid=PMC6372597>, doi: 10.1038/s41386-018-0254-y.
- 791 Noritake A, Nakamura K. Encoding prediction signals during appetitive and aversive Pavlovian conditioning
792 in the primate lateral hypothalamus. *Journal of neurophysiology*. 2019; 121(2):396–417. www.jn.org
793 <http://www.ncbi.nlm.nih.gov/pubmed/30485150>, doi: 10.1152/jn.00247.2018.
- 794 Ogawa SK, Watabe-Uchida M. Organization of dopamine and serotonin system: Anatomical and functional
795 mapping of monosynaptic inputs using rabies virus. *Pharmacology, biochemistry, and behavior*. 2018 nov;
796 174:9–22. <http://www.ncbi.nlm.nih.gov/pubmed/28476484>, doi: 10.1016/j.pbb.2017.05.001.

- 797 **Pollak Dorocic I**, Fürth D, Xuan Y, Johansson Y, Pozzi L, Silberberg G, Carlén M, Meletis K. A Whole-Brain Atlas
798 of Inputs to Serotonergic Neurons of the Dorsal and Median Raphe Nuclei. *Neuron*. 2014; 83(3):663–678.
799 doi: [10.1016/j.neuron.2014.07.002](https://doi.org/10.1016/j.neuron.2014.07.002).
- 800 **Proulx CD**, Aronson S, Milivojevic D, Molina C, Loi A, Monk B, Shabel SJ, Malinow R. A neural
801 pathway controlling motivation to exert effort. *Proceedings of the National Academy of Sciences*.
802 2018 may; 115(22):5792–5797. <http://www.ncbi.nlm.nih.gov/pubmed/29752382><http://www.ncbi.nlm.nih.gov/pmc/articles/PMC5984527/><http://www.pnas.org/lookup/doi/10.1073/pnas.1801837115>, doi:
803 [10.1073/pnas.1801837115](https://doi.org/10.1073/pnas.1801837115).
- 805 **Proulx CD**, Hikosaka O, Malinow R. Reward processing by the lateral habenula in normal and depre-
806 sive behaviors. *Nature Neuroscience*. 2014; 17(9):1146–1152. <http://dx.doi.org/10.1038/nn.3779><http://www.ncbi.nlm.nih.gov/pmc/articles/PMC4305435/>{&}tool=pmcentrez{&}rendertype=abstract, doi:
807 [10.1038/nn.3779](https://doi.org/10.1038/nn.3779).
- 809 **Rosin DL**, Weston MC, Sevigny CP, Stornetta RL, Guyenet PG. Hypothalamic orexin (hypocretin) neurons ex-
810 press vesicular glutamate transporters VGLUT1 or VGLUT2. *The Journal of comparative neurology*. 2003 oct;
811 465(4):593–603. <http://doi.wiley.com/10.1002/cne.10860><http://www.ncbi.nlm.nih.gov/pubmed/12975818>, doi:
812 [10.1002/cne.10860](https://doi.org/10.1002/cne.10860).
- 813 **Scott MM**, Wylie CJ, Lerch JK, Murphy RA, Lobur K, Herlitze S, Jiang W, Conlon RA, Strowbridge BW, Deneris
814 ES. A genetic approach to access serotonin neurons for in vivo and in vitro studies. *Proceedings of
815 the National Academy of Sciences of the United States of America*. 2005; 102(45):16472–16477. doi:
816 [10.1073/pnas.0504510102](https://doi.org/10.1073/pnas.0504510102).
- 817 **Stamatakis AM**, Van Swieten M, Basiri ML, Blair GA, Kantak P, Stuber GD. Lateral Hypothalamic
818 Area Glutamatergic Neurons and Their Projections to the Lateral Habenula Regulate Feeding and Re-
819 ward. *The Journal of neuroscience : the official journal of the Society for Neuroscience*. 2016 jan;
820 36(2):302–11. <http://www.jneurosci.org/cgi/doi/10.1523/JNEUROSCI.1202-15.2016><http://www.ncbi.nlm.nih.gov/pubmed/26758824><http://www.ncbi.nlm.nih.gov/pmc/articles/PMC4710762/>, doi:
821 [10.1523/JNEUROSCI.1202-15.2016](https://doi.org/10.1523/JNEUROSCI.1202-15.2016).
- 823 **Steinmetz NA**, Zatka-Haas P, Carandini M, Harris KD. Distributed coding of choice, action and engage-
824 ment across the mouse brain. *Nature*. 2019 dec; 576(7786):266–273. <http://www.nature.com/articles/s41586-019-1787-x><http://www.ncbi.nlm.nih.gov/pubmed/31776518><http://www.ncbi.nlm.nih.gov/pmc/articles/PMC6913580/>, doi: 10.1038/s41586-019-1787-x.
- 827 **Tervo DGR**, Hwang BY, Viswanathan S, Gaj T, Lavzin M, Ritola KD, Lindo S, Michael S, Kuleshova E, Ojala D,
828 Huang CC, Gerfen CR, Schiller J, Dudman JT, Hantman AW, Looger LL, Schaffer DV, Karpova AY. A Designer
829 AAV Variant Permits Efficient Retrograde Access to Projection Neurons. *Neuron*. 2016; 92(2):372–382. <http://dx.doi.org/10.1016/j.neuron.2016.09.021>, doi: [10.1016/j.neuron.2016.09.021](https://doi.org/10.1016/j.neuron.2016.09.021).
- 831 **Trusel M**, Nuno-Perez A, Lecca S, Takahashi T, Ferraguti F, Correspondence MM. Punishment-Predictive Cues
832 Guide Avoidance through Potentiation of Hypothalamus-to-Habenula Synapses Highlights d Punishments
833 and punishment-predictive cues excite LHB neurons d Avoidance learning strengthens hypothalamus-to-
834 LHB excitation d Hypothalamic. *Neuron*. 2019; p. 1–8. <https://doi.org/10.1016/j.neuron.2019.01.025>, doi:
835 [10.1016/j.neuron.2019.01.025](https://doi.org/10.1016/j.neuron.2019.01.025).
- 836 **Tye KM**. Neural Circuit Motifs in Valence Processing. *Neuron*. 2018; 100(2):436–452. <https://doi.org/10.1016/j.neuron.2018.10.001>, doi: [10.1016/j.neuron.2018.10.001](https://doi.org/10.1016/j.neuron.2018.10.001).
- 838 **Verharen JPH**, Adan RAH, Vanderschuren LJMJ. How Reward and Aversion Shape Motivation and Deci-
839 sion Making: A Computational Account. *The Neuroscientist : a review journal bringing neurobiology,*
840 *neurology and psychiatry*. 2020 feb; 26(1):87–99. <http://www.ncbi.nlm.nih.gov/pubmed/30866712>, doi:
841 [10.1177/1073858419834517](https://doi.org/10.1177/1073858419834517).
- 842 **Warden MR**, Selimbeyoglu A, Mirzabekov JJ, Lo M, Thompson KR, Kim Sy, Adhikari A, Tye KM, Frank LM, Deis-
843 seroth K. A prefrontal cortex-brainstem neuronal projection that controls response to behavioural chal-
844 lenge. *Nature*. 2012 dec; 492(7429):428–32. <http://www.nature.com/articles/nature11617><http://www.ncbi.nlm.nih.gov/pubmed/23160494><http://www.ncbi.nlm.nih.gov/pmc/articles/PMC5929119/>, doi:
845 [10.1038/nature11617](https://doi.org/10.1038/nature11617).
- 847 **Weissbourd B**, Ren J, DeLoach KE, Guenthner CJ, Miyamichi K, Luo L. Presynaptic Partners of Dorsal Raphe
848 Serotonergic and GABAergic Neurons. *Neuron*. 2014; 83(3):645–662. <http://dx.doi.org/10.1016/j.neuron.2014.06.024>, doi: [10.1016/j.neuron.2014.06.024](https://doi.org/10.1016/j.neuron.2014.06.024).

- 850 Zhang ZM, Chen S, Liang YZ. Baseline correction using adaptive iteratively reweighted penalized least squares.
851 The Analyst. 2010 may; 135(5):1138-46. <https://github.com/zmzhang/airPLS><http://www.ncbi.nlm.nih.gov/pubmed/20419267>, doi: 10.1039/b922045c.
- 853 Zhou L, Liu MZ, Li Q, Deng J, Mu D, Sun YG. Organization of Functional Long-Range Circuits Controlling the
854 Activity of Serotonergic Neurons in the Dorsal Raphe Nucleus. Cell Reports. 2017; 18(12):3018–3032. <http://linkinghub.elsevier.com/retrieve/pii/S2211124717302954>, doi: 10.1016/j.celrep.2017.02.077.
- 855

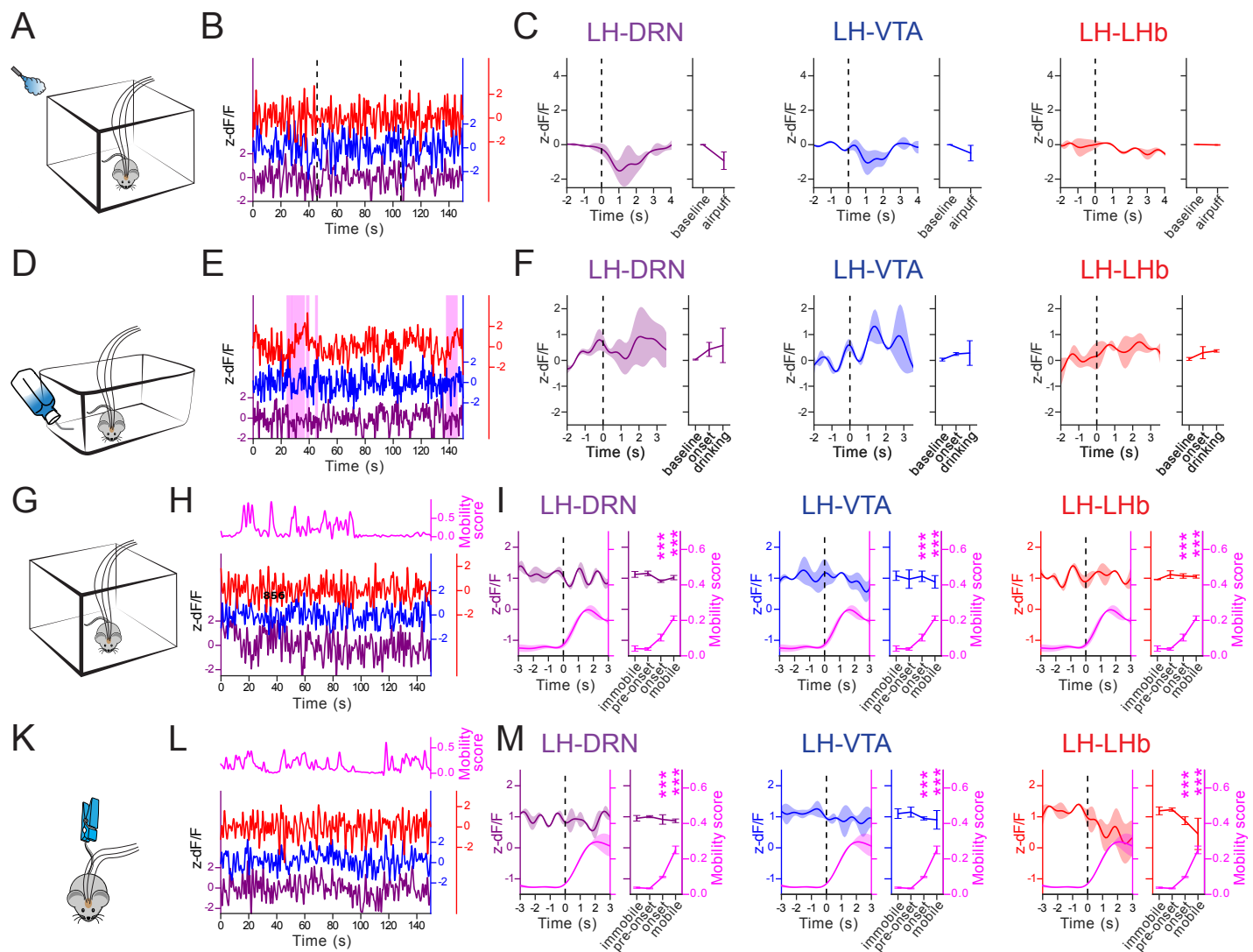


Figure 1–Figure supplement 1. Recordings from the LH→DRN, LH→VTA, and LH→LHb pathways of control eYFP-expressing mice. **(A)** Diagram of the experimental setup for the airpuff. **(B)** Representative signal traces associated to the airpuffs (dashed vertical bars) simultaneously measured at the LH→DRN, LH→VTA, and LH→LHb pathways. **(C)** Peri-event plot of the average signals to all the airpuff events at the LH→DRN, LH→VTA, and LH→LHb pathways. Plot for average response before and after airpuffs. Lines represent mean ± SEM. Same convention as **D–F** for sucrose consumption test (**G–I**), open field test (**K–M**), and tail suspension test (**N–P**). The sucrose consumption events are represented by pink shaded box in **H**. The magenta lines are the mobility scores. The statistical analysis was performed along with the data from the mice expressing GCaMP6s.

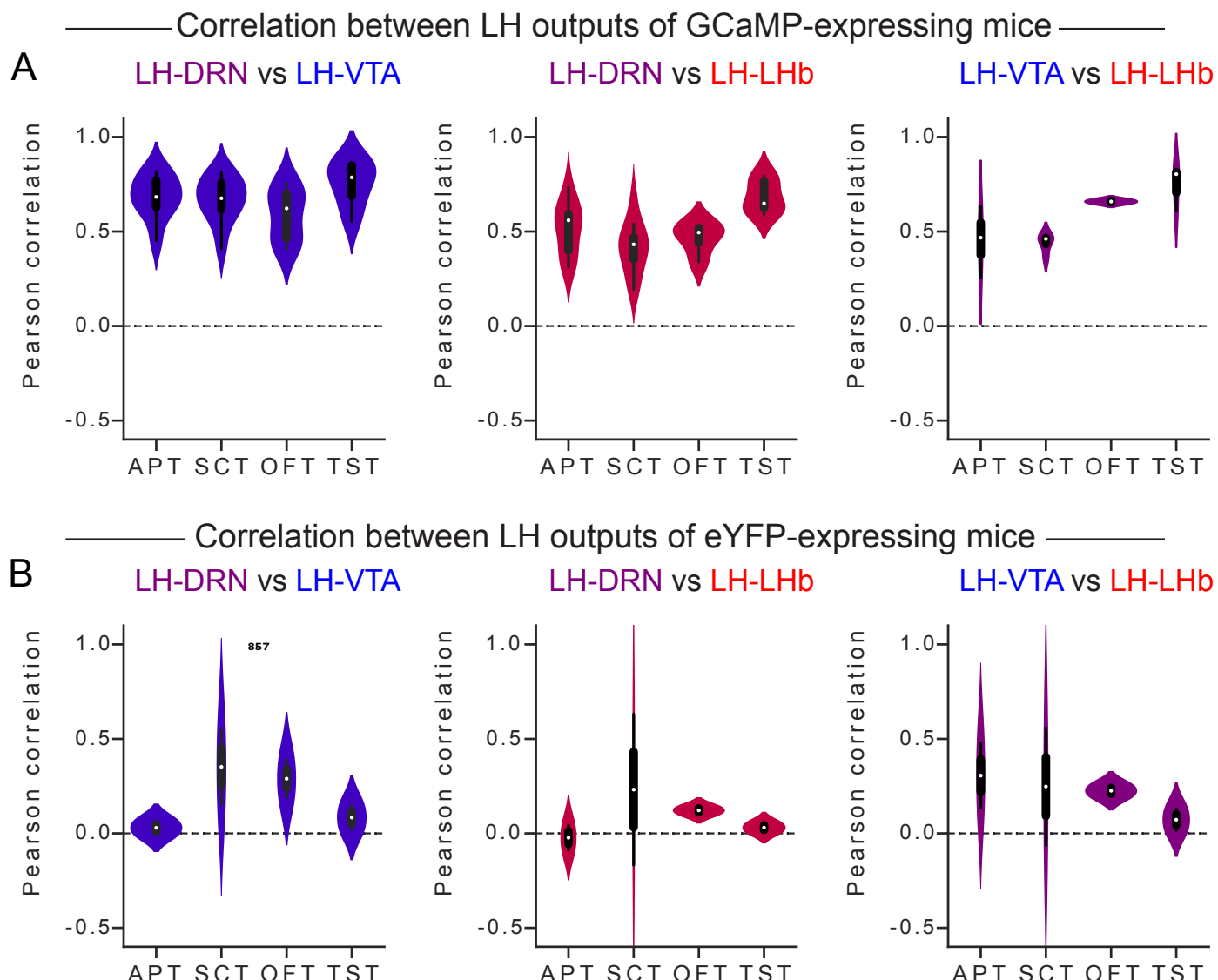


Figure 1-Figure supplement 2. Pearson correlation between the signals recorded at the LH \rightarrow DRN, LH \rightarrow VTA, and LH \rightarrow LHb pathways in mice expressing GCaMP6s and eYFP. **(A)** Pearson correlation between the Ca^{2+} signals recorded at the LH \rightarrow DRN, LH \rightarrow VTA, and LH \rightarrow LHb pathways in mice expressing GCaMP6s. **(B)** Pearson correlation between the Ca^{2+} signals recorded at the LH \rightarrow DRN, LH \rightarrow VTA, and LH \rightarrow LHb pathways in mice expressing eYFP. Three-way ANOVA between factors group (GCaMP6s- and eYFP-expressing mice), and within factors pathway (LH \rightarrow DRN, LH \rightarrow VTA, and LH \rightarrow LHb), and tests (APT, airpuff test; SCT, sucrose consumption test; OFT, open field test; TST, tail suspension test) with post hoc Tukey test. The p values were adjusted using the Bonferroni multiple testing correction method. The main effect was the difference between the mice expressing GCaMP6s and eYFP ($p < 0.05$). One sample t-test showed significant difference from 0 in mice expressing GCaMP6s ($p < 0.05$), but not in mice expressing eYFP ($p > 0.2$)

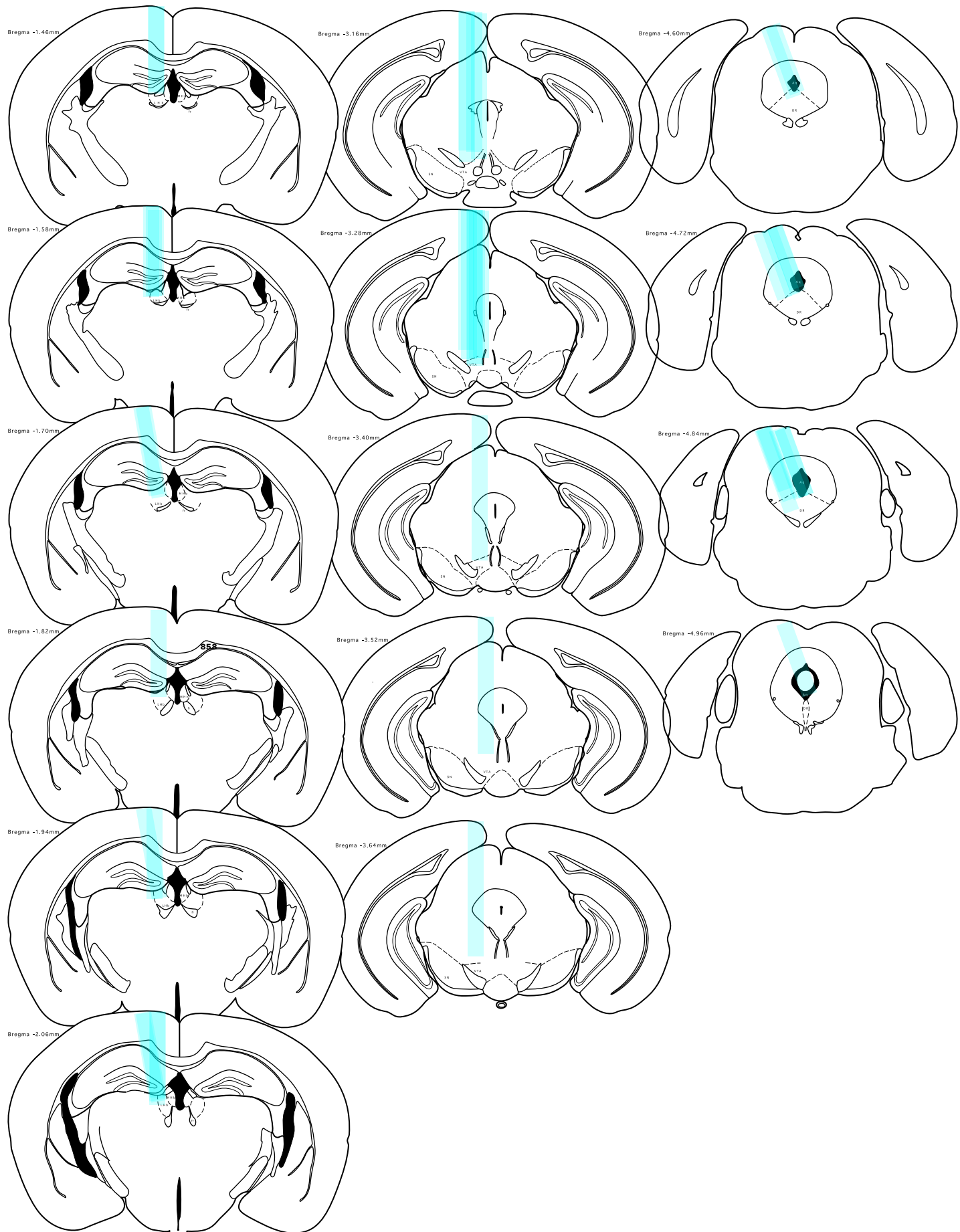


Figure 1-Figure supplement 3. Cannulae placement in mice expressing GCaMP6s in the LHB (**left**), the VTA (**middle**), and the DRN (**right**)

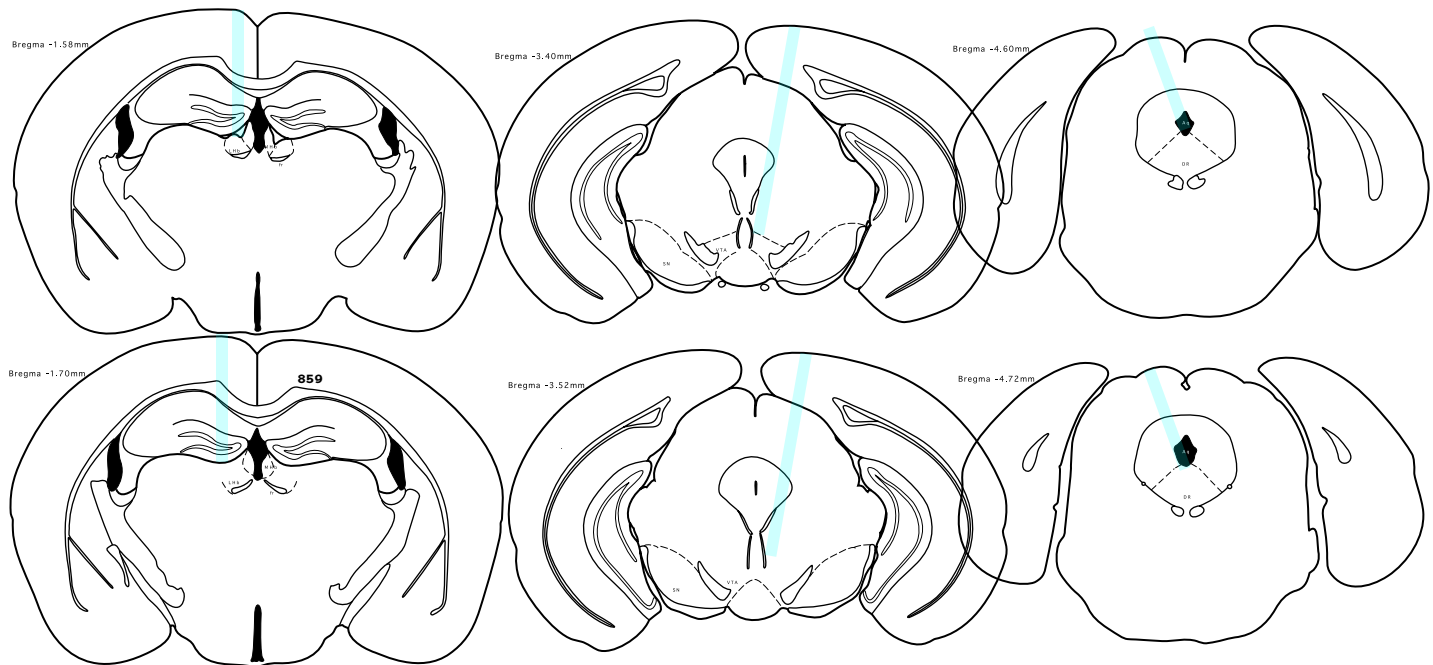


Figure 1-Figure supplement 4. Cannulae placement in the mice expressing eYFP in the LHb (**left**), the VTA (**middle**), and the DRN (**right**)

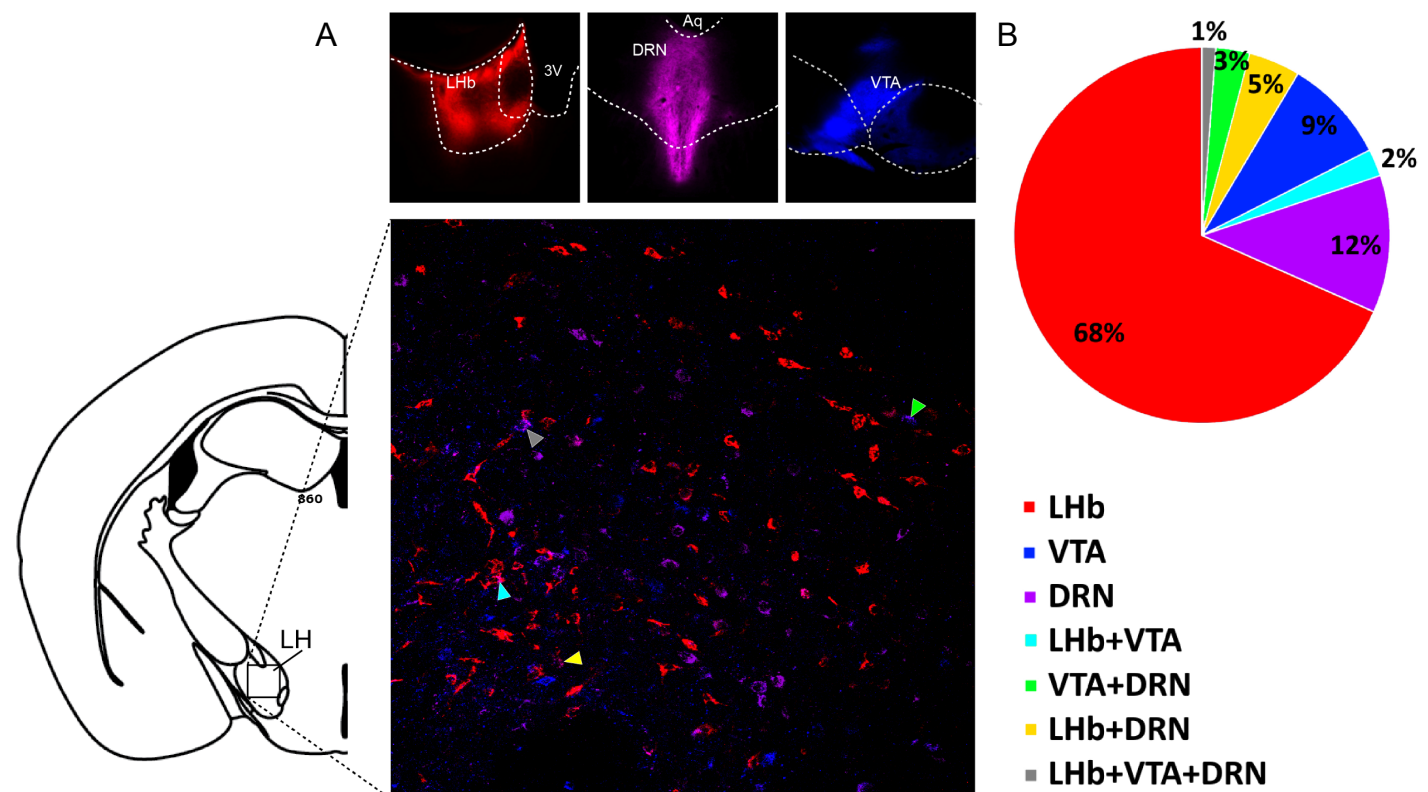


Figure 1-Figure supplement 5. The LH neural populations projecting to the DRN, VTA, and LHb are largely distinct populations. **(A)** Representative fluorescent images of the fluorescent markers CTx 488, CTx 594, and CTx 647 (CTx – Cholera toxin) injected in the DRN, the VTA, and the LHb (top panels), and representative confocal image of LH neurons positive for markers (bottom panel). Images are pseudo colored. **(B)** Pie chart representing the relative fraction of labeled LH neurons projecting to either the DRN, VTA, or LHb, and their co-localization.

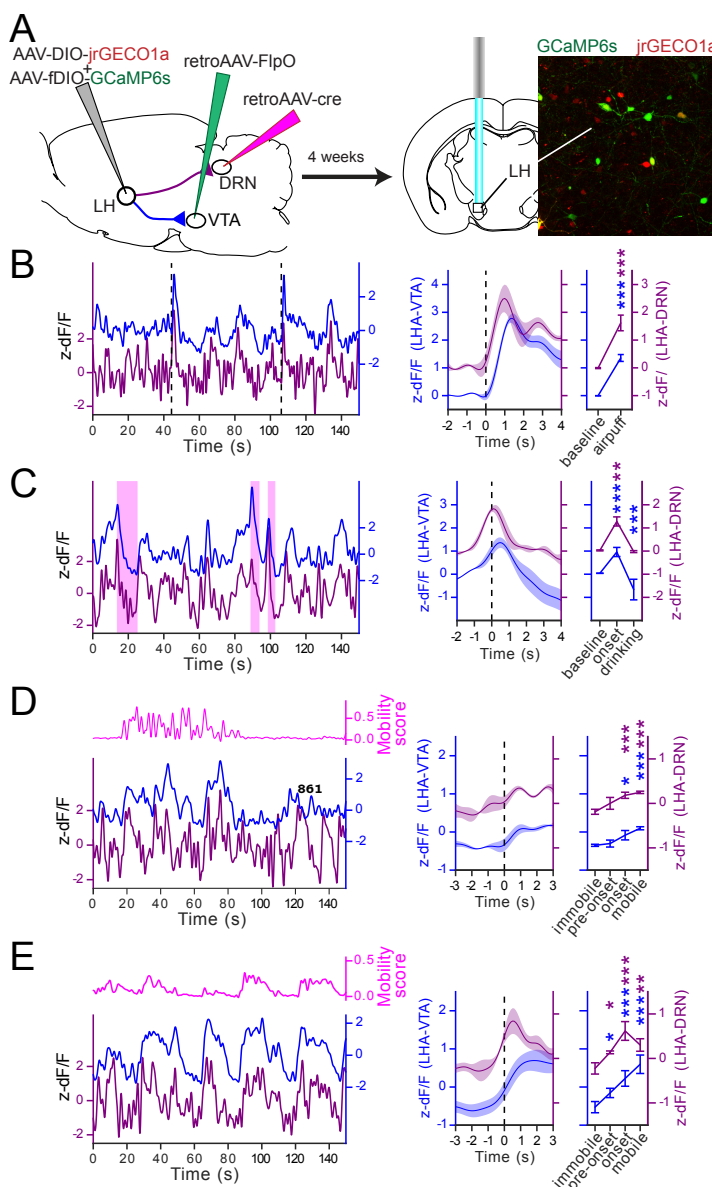


Figure 1-Figure supplement 6. Ca^{2+} imaging from the LH neurons projecting to the DRN and the VTA. **(A)** Diagram of the experimental setup and representative fluorescent image of LH neuron expressing GCaMP6s (green) and jrGECO1a (red) projecting to the VTA and DRN, respectively. **(B)** Representative Ca^{2+} signal traces associated with the airpuffs (dashed vertical bars) simultaneously measured from the LH neurons expressing GCaMP6s (projecting to the VTA) and jrGECO1a (projecting to the DRN) (**left**). Peri-event plot of the average Ca^{2+} signals to all the airpuff events at the LH \rightarrow DRN and LH \rightarrow VTA LH neurons, and plot of the average responses before and after the airpuffs (**right**). Lines represent the means \pm SEM. Same convention as for **B** for the sucrose consumption test (**C**), the open field test (**D**), and the tail suspension test (**E**). The sucrose consumption events are represented by the pink shaded boxes in **C**. The magenta lines are the mobility scores. Repeated measures two-way ANOVA within factors pathways (LH \rightarrow DRN and LH \rightarrow VTA) and time periods (different for each test) with post hoc Dunnett's test. The *p* values were adjusted using the Bonferroni multiple testing correction method. **p* < 0.05, ***p* < 0.01, ****p* < 0.001.

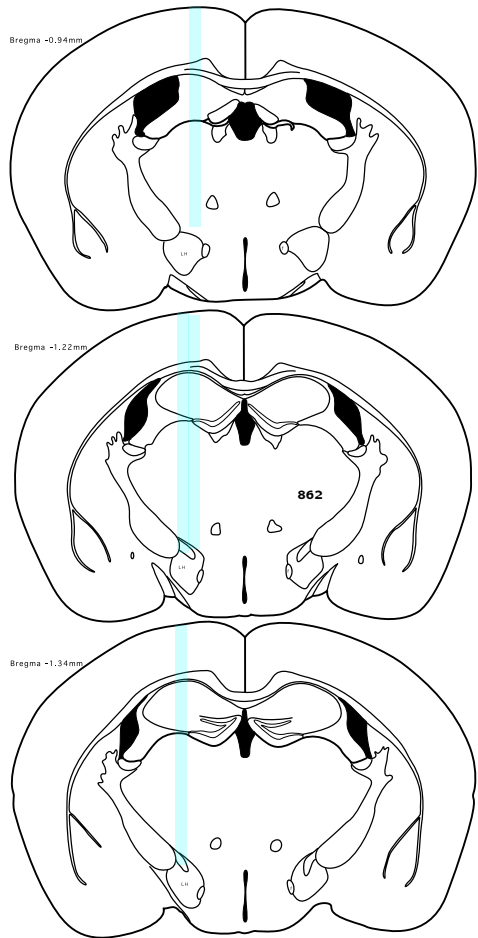


Figure 1–Figure supplement 7. The cannulae placement in mice prepared using the intersectional viral strategy

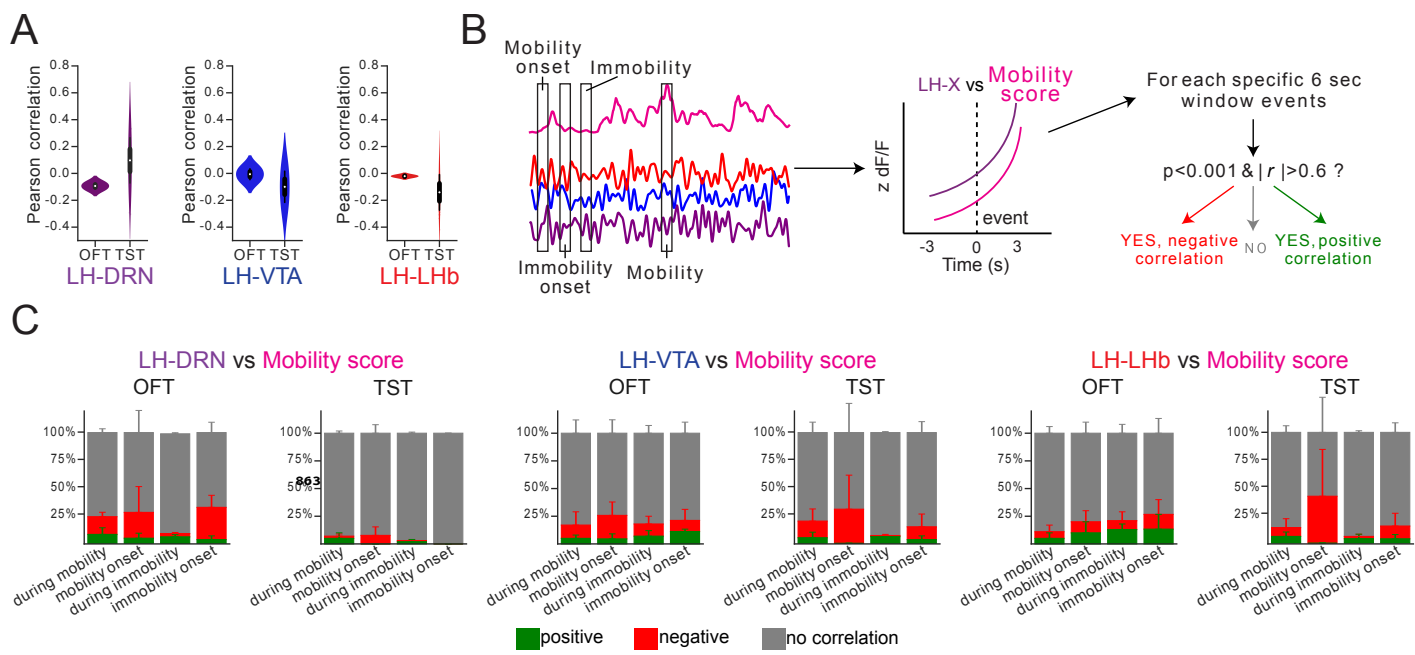


Figure 2–Figure supplement 1. Correlation analysis between the signal at one of the LH neural output pathways and mobility score in mice expressing eYFP.. **(A)** The Pearson correlation between the Ca^{2+} signal measured at the LH \rightarrow DRN, LH \rightarrow VTA, and LH \rightarrow LHb pathways and the mobility score during a complete session in the OFT or the TST. **(B)** Schematic of the event selection. Events at the onset of mobility and immobility and random events during mobility and immobility were chosen, and the Pearson correlation at 6-seconds peri-events between the Ca^{2+} signal and the mobility score was calculated. Correlations with $p < 0.001$ and $|r| > 0.6$ were considered as positive, $p < 0.001$ and $|r| < 0.6$ – negative, the others – not correlated. **(C)** Fraction of positive (green), negative (red), and uncorrelated events (gray) in the OFT and TST for the LH \rightarrow DRN, LH \rightarrow VTA, and LH \rightarrow LHb pathways. Statistical analysis was performed along with the data from the mice expressing GCaMP6s.

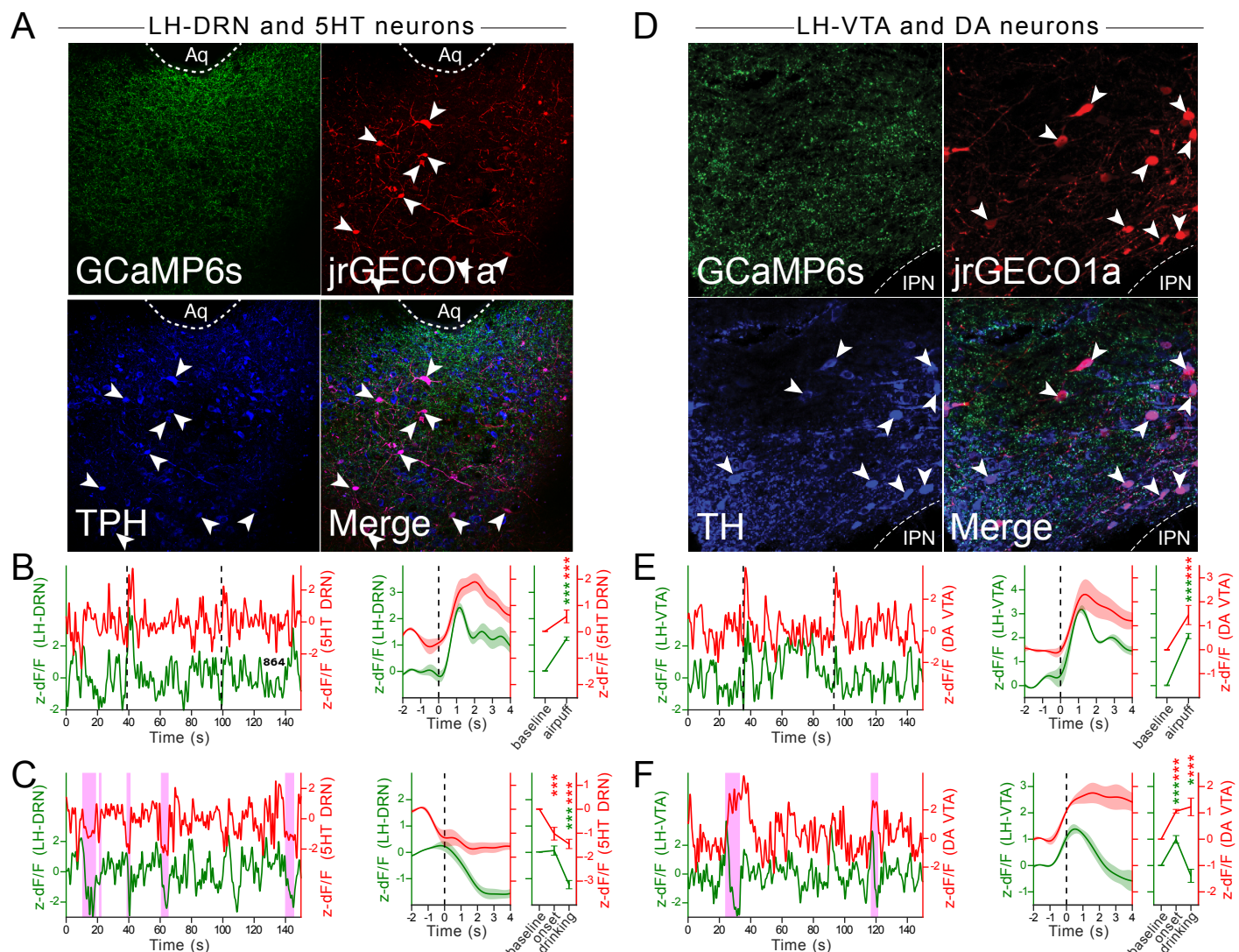


Figure 3–Figure supplement 1. Simultaneous recordings at the DRN^{5HT} neurons and the LH \rightarrow DRN pathway, and at the VTA^{DA} neurons and the LH \rightarrow VTA pathway in the AP and the SCT. **(A, D)** Confocal images of the DRN neurons **(A)** and VTA neurons **(D)** expressing jrGECO1a and immunolabelled for the serotoninergic marker tryptophane hydroxylase (TPH, blue **A**) or the dopaminergic marker tyrosine hydroxylase (TH, blue **D**). Shown in green are the LH axon terminals in the DRN and VTA that are expressing GCaMP6s. Representative Ca^{2+} signal traces recorded from the DRN^{5HT} neurons and at the LH \rightarrow DRN pathway **(B)** or from the VTA^{DA} neurons and at the LH \rightarrow VTA pathway **(E)** in mice presented with airpuffs **(B, E) (left)**. Peri-event plots of the average Ca^{2+} signal traces with all the onset of mobility and the plots for the AUC at baseline and after the airpuffs **(right)**. The lines represent means \pm SEM. Same convention as for **B, E** for the SCT **(C, F)**. Repeated measures two-way ANOVA within factors pathways (DRN^{5HT} and LH \rightarrow DRN or VTA^{DA} and LH \rightarrow VTA) and time periods (during immobility and mobility, at mobility pre-onset and onset) with post hoc Dunnett's test. The p values were adjusted using the Bonferroni multiple testing correction method. * p < 0.05, ** p < 0.01, *** p < 0.001.

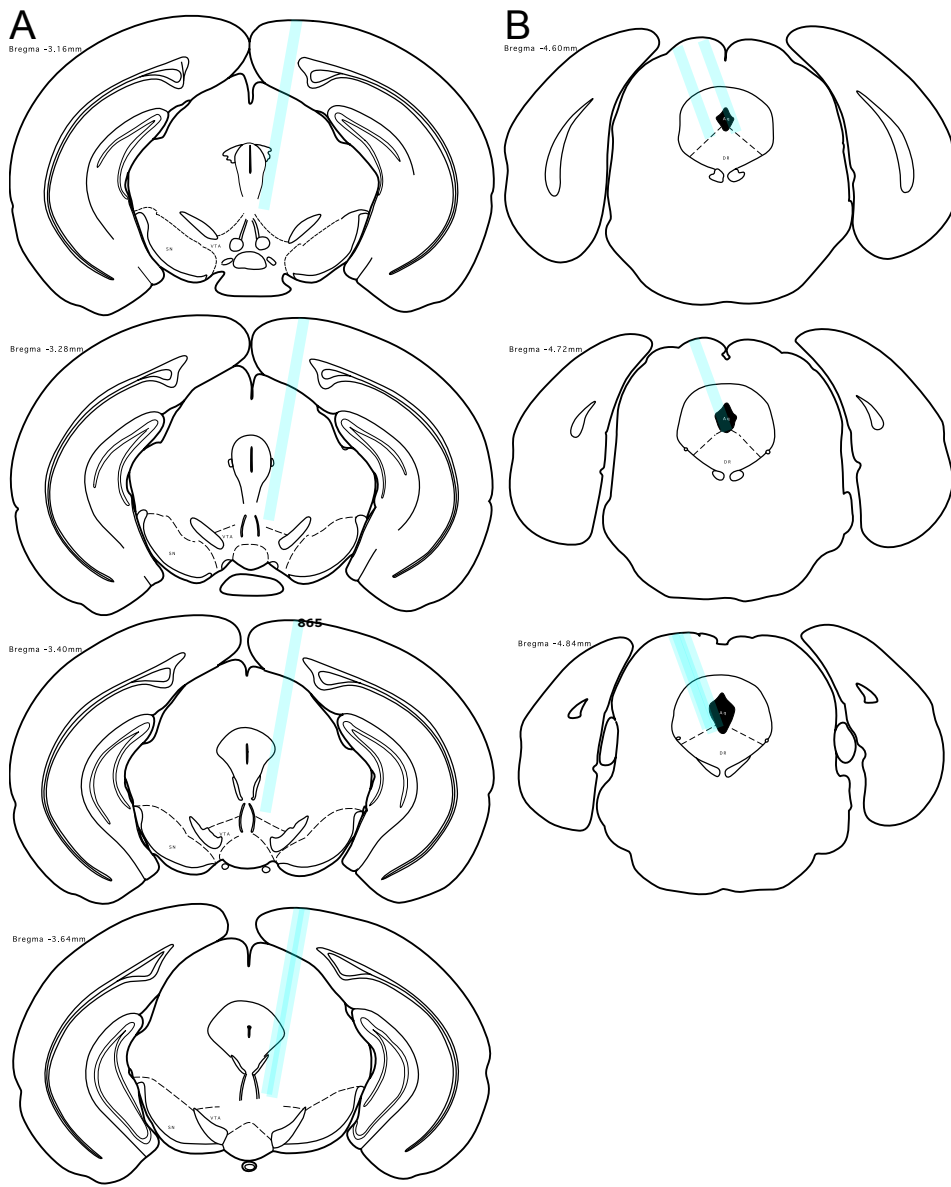


Figure 3-Figure supplement 2. Cannulae placement in the ePet-cre (**A**) and DAT-ires-cre (**B**) mice

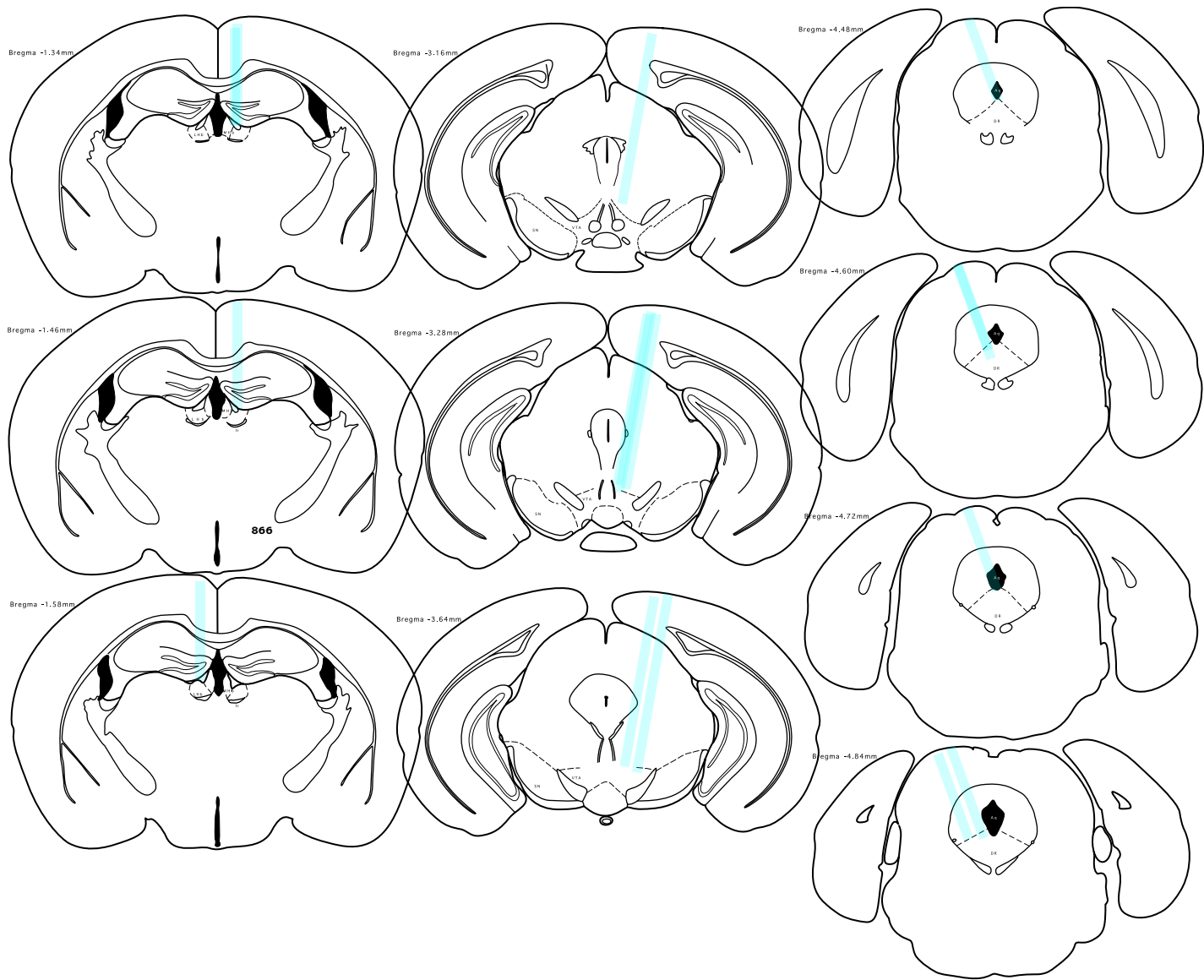


Figure 4-Figure supplement 1. Cannulae placement in the LHB (**left**), the VTA (**middle**), and the DRN (**right**) of mice tested in the active avoidance task.

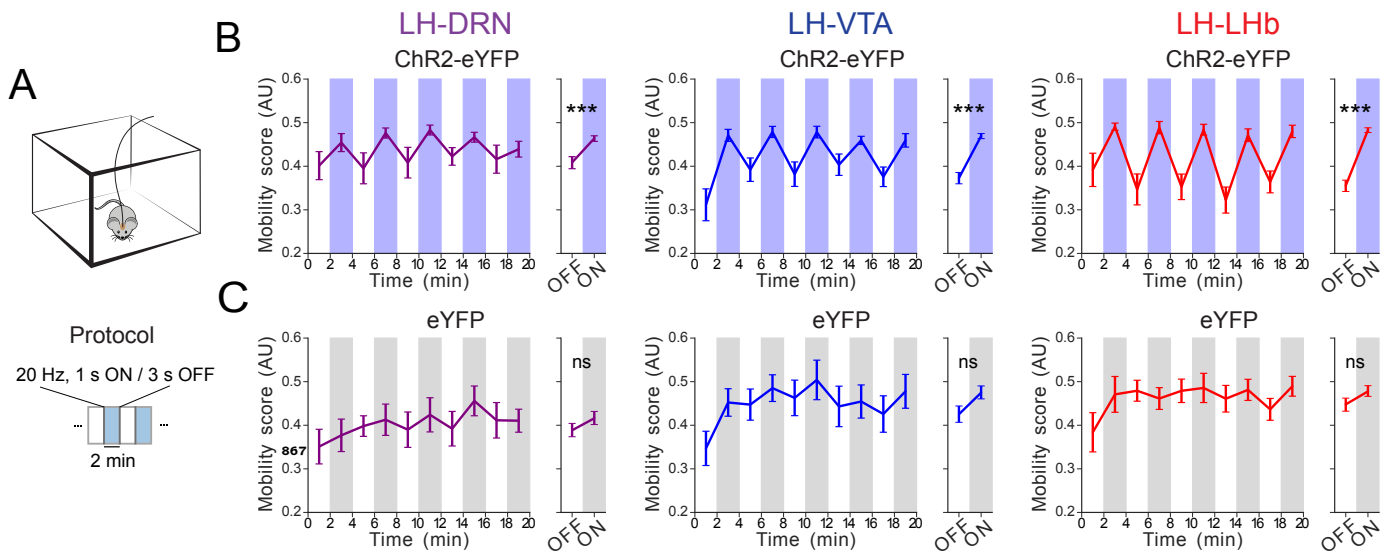


Figure 6-Figure supplement 1. Optostimulation of the LH→DRN, LH→VTA, or LH→LHb pathways in the OFT. **(A)** Diagram of the experimental protocol for the OFT. The mobility of the mice was evaluated during a 20 min OFT session with alternating 2-min epochs without or with 1-s, 20 Hz trains every 4 sec. Mobility was automatically monitored with a video tracking system. **(B-C)** Plots of mean mobility (mean \pm SEM) during periods of optogenetic stimulation (blue (**C**) or gray (**D**)) or no light (white) at the LH→DRN (**left**), LH→VTA (**middle**), or LHA→LHb (**right**) pathways in ChR2-eYFP- (**C**) and eYFP-expressing (**D**) mice. Four-way repeated measures ANOVA between factors of group (ChR2-eYFP- and eYFP-expressing mice), and within factors pathway (LH→DRN, LH→VTA, or LH→LHb), time period (five 4-minutes periods) and laser (on and off) with post hoc Tukey test. The *p* values were adjusted using the Bonferroni multiple testing correction method. **p* < 0.05, ***p* < 0.01, ****p* < 0.001, *p* > 0.2 ns (not significant).

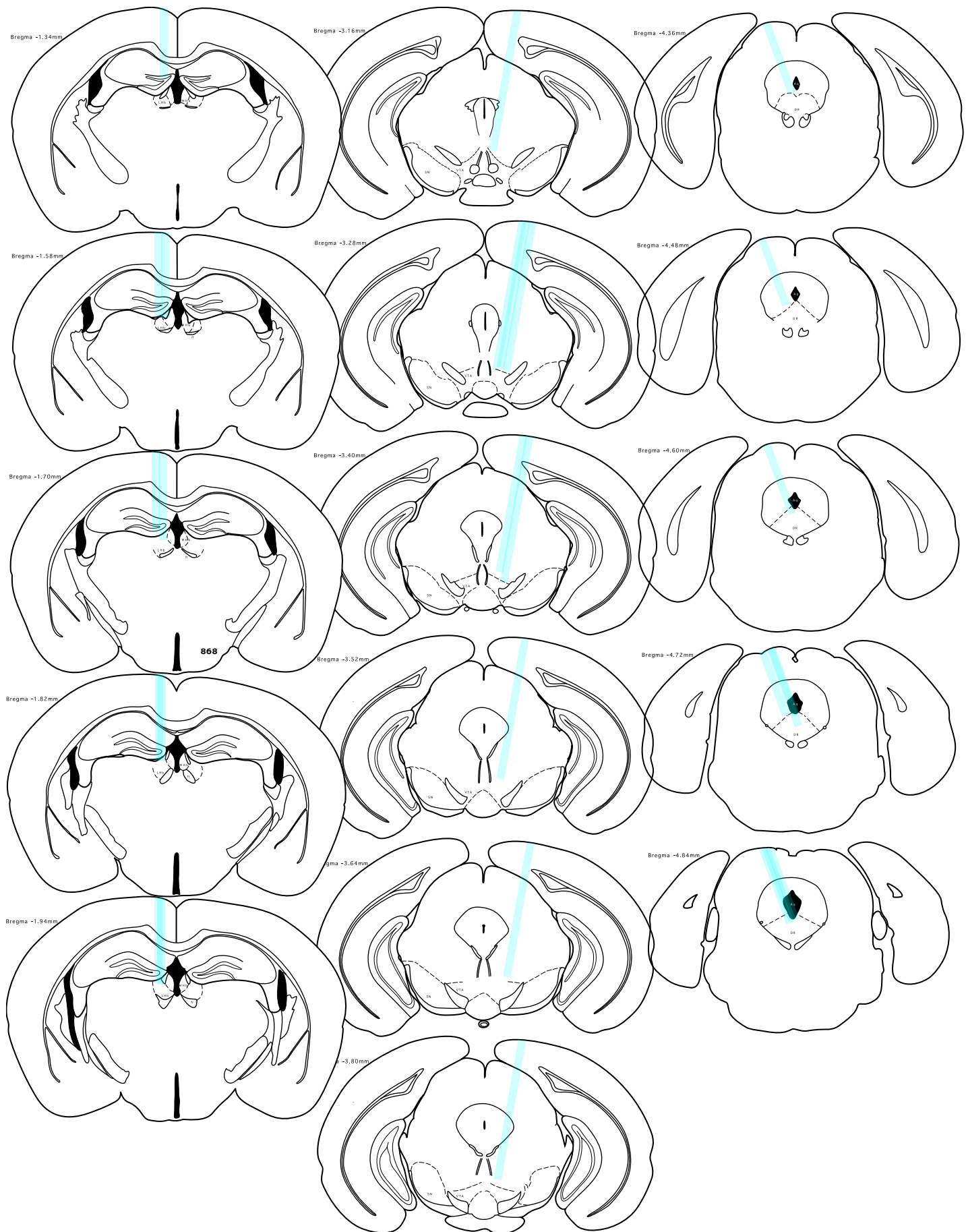


Figure 6-Figure supplement 2. Cannulae placement in the LHB (**left**), the VTA (**middle**), and the DRN (**right**)in mice expressing ChR2-eYFP

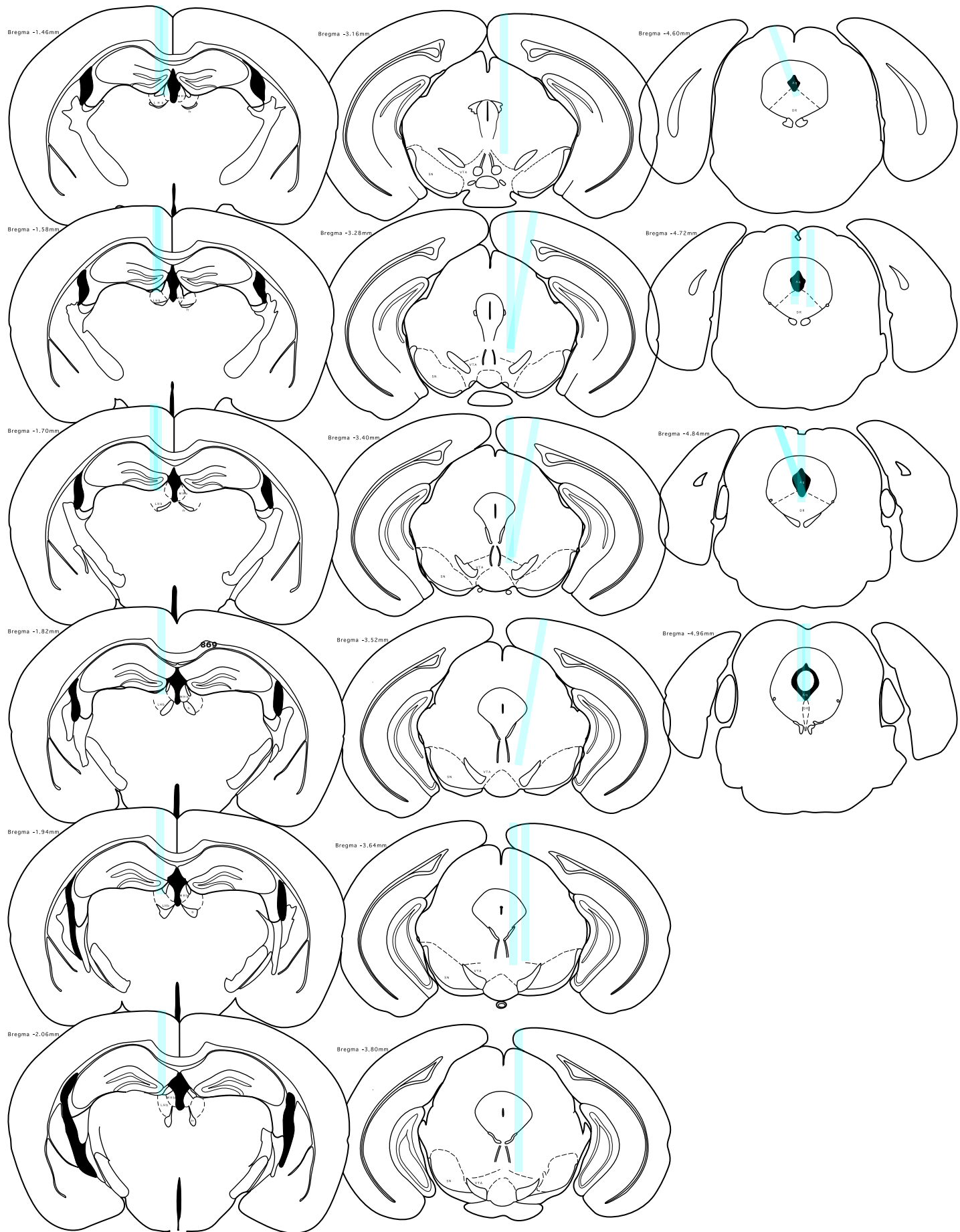


Figure 6-Figure supplement 3. Cannulae placement in the LHB (**left**), the VTA (**middle**), and the DRN (**right**)in mice expressing eYFP

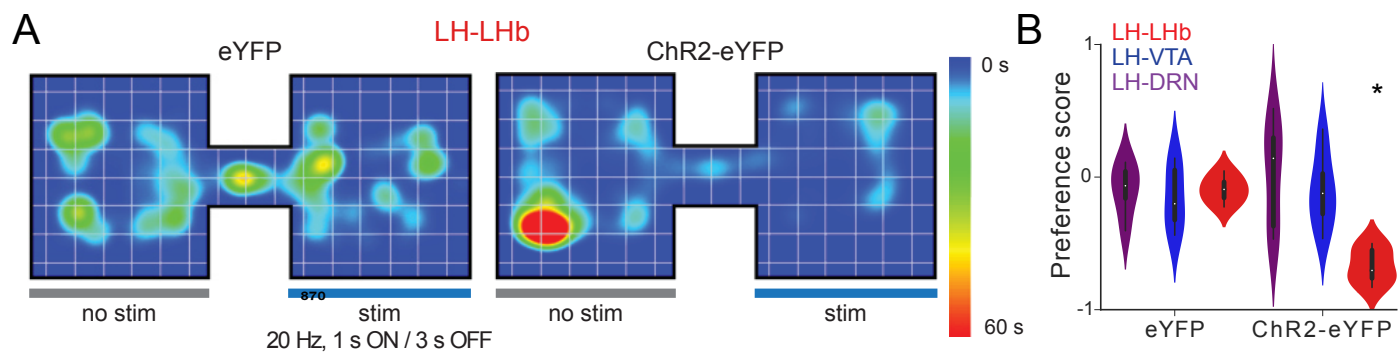


Figure 7-Figure supplement 1. Optostimulation of the LH→DRN, LH→VTA, or LH→LHb pathways in the RTPP and the SCT. **(A)** The heatmaps of animal location in the RTPP during optostimulation of the LH→LHb pathway in mice expressing ChR2-eYFP (**left**) or eYFP (**right**). **(B)** The preference scores measured in the RTPP during optostimulation of the LH→DRN, LH→VTA, or LH→LHb pathways in mice expressing ChR2-eYFP or eYFP. Two-way ANOVA between factor of group (ChR2-eYFP- and eYFP-expressing mice) and within factor pathway (LH→DRN, LH→VTA, or LH→LHb) with post hoc Tukey test. The *p* values were adjusted using the Bonferroni multiple testing correction method. #*p* < 0.1, **p* < 0.05, ***p* < 0.01, ****p* < 0.001, ns (not significant) – *p* > 0.2.